NUMERICAL SIMULATION OF METHANE-AIR DDT IN CHANNELS CONTAINING TRACE AMOUNTS OF IMPURITIES

A Thesis

by

LOGAN NASH KUNKA

Submitted to the Office of Graduate and Professional Studies of
Texas A&M University
in partial fulfillment of the requirements for the degree of

MASTER OF SCIENCE

Chair of Committee,	Elaine Oran
Committee Members,	Eric Petersen
	Waruna Kulatilaka
Head of Department,	Srinivas Rao Vadali

May 2021

Major Subject: Aerospace Engineering

ABSTRACT

Accidental explosions in industrial and military settings often cause devastating losses to personnel and infrastructure. Many of these events, such as those in coal mines or fuel processing and transport, are attributed to the accumulation natural gas, which consists of methane with trace amounts impurities which are usually heavier hydrocarbon gases. These heavy hydrocarbons, such as propane (C_3H_8) and ethane (C_2H_6), are usually found in trace amounts of up to 20% by volume. These fuels mix with air, create conditions for flame ignition, and subsequently may lead to a deflagration-to-detonation transition (DDT). This research discusses the conditions under which flames in idealized channel geometries can accelerate to detonation. DDT was investigated for the addition of ethane and propane into a methane-air mixture at various geometry scales with constant blockage ratio and channel configuration. Simulations of small channels containing natural gas were compared with existing experimental data. We found that the location where DDT occurred, L_{DDT}, decreased only slightly as the percentage of impurity changed. The variation was, in fact, on the order of uncertainly due to turbulence and turbulence interactions (i.e., the stochasticity) in the simulation. The simulations do suggest a decrease in detonation cell size with increased impurity, which would result in a more robust detonation wave.

DEDICATION

To my family and friends. I am grateful for your unconditional support throughout the years.

ACKNOWLEDGMENTS

I would like acknowledge and thank Dr. Elaine Oran for allowing me to continue my graduate education. Through her guidance as a professor and advisor, she has helped me develop as a scholar and increase my knowledge exponentially during the past few years. I would like to thank my fellow researchers and colleagues Ashwath Venkataraman, Nathan Gaddis, Xiao Zhang, Xiaoyi Lu, and Zhenyang Dong. Specifically, I would like to thank Dr. Carolyn Kaplan, Dr. Vadim Gamezo, and Christian Bachman for their support in this research.

CONTRIBUTORS AND FUNDING SOURCES

Contributors

This work was supported by a thesis committee consisting of Professor Elaine Oran of the Department of Aerospace Engineering and Professors Eric Petersen and Waruna Kulatilaka of the Department of Mechanical Engineering.

The data analyzed in Section 2.3 was provided by Dr. Carolyn Kaplan and data from ALLA simulations were provided by Dr. Vadim Gamezo. All other work conducted for the thesis was completed by the student independently.

Funding Sources

Graduate study was supported by the Alpha Foundation and DOE Computational Science Graduate Fellowship. Computing resources were provided by Texas A&M High Performance Research Computing and the Department of Defense High Performance Computing Modernization Program.

TABLE OF CONTENTS

Page

LIST OF FIGURES

FIGURE Page

LIST OF TABLES

1. INTRODUCTION*

1.1 Introduction

Accidental explosions are rare events but are devastating when they occur. These accidents are a safety concert to various industries including oil and gas, mining, military, and fuel refining and transportation [6, 7, 8, 9]. For the mining industry in particular, the conditions for such explosions are created in confined regions of underground mines such as abandoned and sealed sections of the mine. Natural gas can accumulate in these sealed sections mixing with air to create an explosive gas mixture. This was the case for the Sago Mine explosion in 2006.

Historically, studies of detonation behavior were motivated by industries prone to uncontrolled or accidental explosions and those trying to find practical applications for aerospace or military purposes. Detonations differ from low-speed flames, or deflagrations, primarily through the coupling of the combustion process with a strong shock [10]. Detonations are characterized, most notably, by their supersonic wave velocity and detonation cell size. Detonation cells are the result of transverse waves in the detonation front causing diamond like patterns across a surface. The size of these cells are generally an indicator of the detonability of the gas. While it is possible to trigger detonation through the deposition of large amounts of energy [10], these ignition sources are not common. Explosions are generally created through the ignition of a fuel-air mixture that begins as a deflagration or low-speed flame. Under certain conditions, this deflagration can accelerate to detonation in a process known as deflagration-to-detonation-transition (DDT). DDT is due to the complex interaction of flame, shocks, boundary layers, and turbulence which include a variety of physical and chemical processes [11].

If detonation occurs in accidental explosions, the destructive potential of the explosion increases enormously. When DDT occurs in the system, the energy release rate drastically increases

*Parts of this section is reprinted from "Numerical simulation of methane-air DDT in channels containing trace amounts of impurities" with permission from Kunka, L.N., Proceedings of the Mary Kay O'Connor Process Safety Symposium, College Station, TX, 2020, and from "Numerical simulations of flame acceleration and DDT in natural gas: the effects of trace propane and ethane" with permission from Kunka, L.N., 2020 American Physical Society Division of Fluid Dynamics, Chicago, IL, 2020.

and the resulting detonation wave can travel at several kilometers per second. The explosion frequently has the same pathway: ignition, flame propagation and acceleration, then transition to detonation. The path to detonation is the response of a reactive gas to a smaller explosions created in deflagration or from the formation of hotspots [11, 12]. Goodwin et. al [13] and Xiao et. al [14] showed that DDT can also occur through shock focusing on the flame front or the unburnt mixture ahead of the flame. It is important to know the distance it takes for such DDT process to occur so that protective seals can be designed accordingly [15].

Detonation is not necessarily unwanted, however. In many aerospace applications, these detonations can be used as a more efficient method to provide thrust for aircraft propulsion. Pulse Detonation Engines (PDE) are an example of such technology. PDEs can use DDT as a mechanism to trigger detonation rather than directly deposit large amounts of energy in the fuel-air mixture. To trigger detonation through DDT, the Shchelkin spiral is often used. The same fundamental understanding of detonation physics is key to advancing both safety science and future propulsion technologies.

Previous research focusing on such explosions has modeled the explosive mixture as pure methane-air [16, 17, 18]. While the primary hydrocarbon in natural gas is methane, often there are trace amounts of impurities such as propane and ethane. These heavier hydrocarbons are often 0-20% of natural gas by volume. The objective of this study is to understand the influence of these impurities on the DDT process and ultimately how it effects the run-up distance to the onset of DDT (L_{DDT}).

Typical Composition of Natural Gas		
Methane	CH_4	70-90%
Ethane	C_2H_6	0-20%
Propane	C_3H_8	
Butane	C_4H_{10}	
Carbon Dioxide	CO_2	0-8%
Oxygen	O_2	0-0.2%
Nitrogen	N_2	0-5%
Hydrogen Sulphide	H_2S	0-5%
Rare Gases	A, He, Ne, Xe	trace

Table 1.1: Realistic natural gas composition.

The following sections of this thesis provide a brief literature review on the DDT in channels from both experimental investigations and numerical simulations. Additionally, a short review of previous work in fuel mixtures is detailed. Following this, a description of the numerical algorithms and chemical reaction models used is this work are outlined. Next, the physics of reacting flow for simplified deflagration and detonation wave are presented. The insights from these phenomena are key to developing the simplified chemical models as well as understanding the large scale system behavior of reacting flows. Simulations of these full-scale systems for idealized channels with two types of obstacles are presented next. Lastly, we conclude with the analysis of the results as well as a discussion and recommendations for future work.

1.2 Literature Review

The earliest studies in understanding detonations goes back to 1883 to the work Mallard and Le Chatelier [19]. They pioneered research in uncontrolled explosions, particularly explosions in mines that were relevant at the time. Over a century later, these types of explosions still remain a problem.

1.2.1 DDT in Idealized Channels

Ciccarelli and Dorofeev [20] summarized many previous experiments on flame acceleration and DDT in smooth ducts and ducts with obstacles. They discuss the physical mechanism for DDT and under which conditions to expect DDT. They show that the onset of DDT is a local phenomenon that is technically separate from the flame acceleration where turbulent combustion plays a key role. However, the flame acceleration is important as it creates the conditions for DDT to occur. Obstacles and geometric configurations dictate the rate of turbulence generation which creates fast flames.

For channels with obstacles, previous computational work has shown effects of blockage ratio, obstacle type, and obstacle placement on the distance to DDT (L_{DDT}) [21, 22]. Gamezo et al. [23] studied the geometric effect of obstacles in hydrogen-air mixtures with difference channel widths d and obstacle spacing d with $BR = 0.5$. They found the time and length to DDT to increase linearly with d^2. In a separate publication [24], they examined the effect of obstacle spacing on flame acceleration and DDT. For channels with higher obstacle density, the flame accelerates more quickly due to the increased perturbation wrinkling the flame and creating more flame surface area. Additionally, DDT can occur when the obstacle are spaced far enough apart for Mach stems to form.

Kuznetsov et al. [1] investigated DDT in methane-air mixtures for 17.4cm and 52cm channels with blockage ratio (BR) or 0.3 and 0.6. BR is the ratio of orifice diameter d to channel inner diameter D. Experiments were carried out at atmospheric conditions with 99.9% pure CH_4 at 5.5 to 17% concentration by volume. They showed a critical diameter $d/\lambda \approx 1$ for $BR = 0.3$ and critical length $L/\lambda \approx 7$. Where λ is the detonation cell size, d is the channel diameter, and L is the axial length down the channel. Flame velocity vs. distance for BR of 0.3 and 0.6 are shown in Figure 1.1.

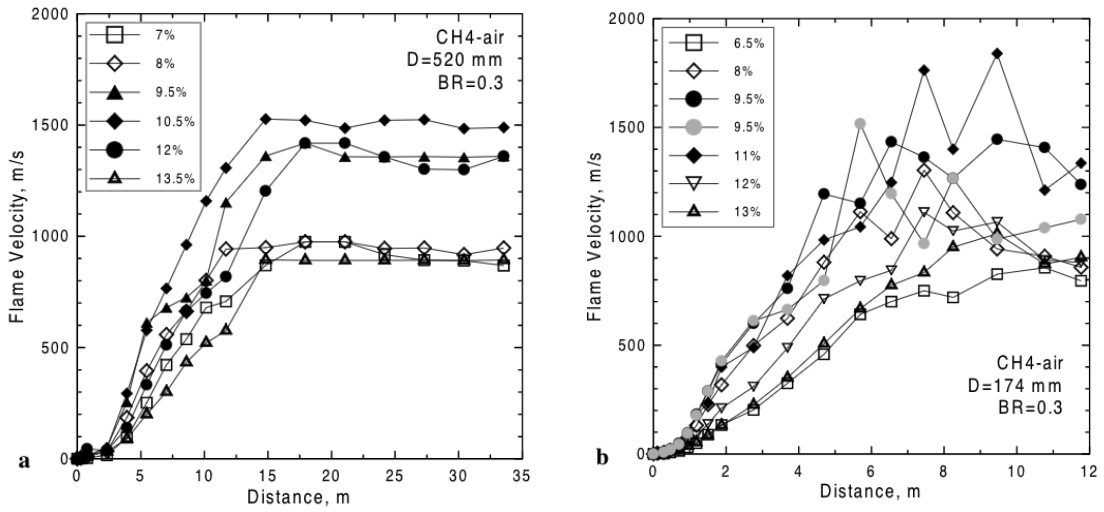

Figure 1.1: DDT in methane-air mixtures. Reprinted from [1]

Zipf et al. [2] and Gamezo et al. [3] performed experimental studies on natural-gas DDT with the Gas Explosions Test Facility (GETF) at the NIOSH Lake Lynn Laboratory. The GETF used a 105cm diameter tube at 73.2m long. Using a baffles spaces 1.52m apart, they tested blockage ratios of 0.13, 0.25, and 0.5. They observed DDT in the obstacle section for compositions ranging from 8.0% to 10.9% NG-air. They noted most cases sustained a detonation beyond the baffles in the smooth section of the tube. DDT was seen for all BR tested. Figures **??** and **??** summarize their results. X_{ru} is the run-up length where shock velocity and flame velocity are greater than 800m/s and shock pressure is greater than 1MPa. X_{DDT} is the location of DDT after X_{ru} where shock pressure exceeds 2MPa.

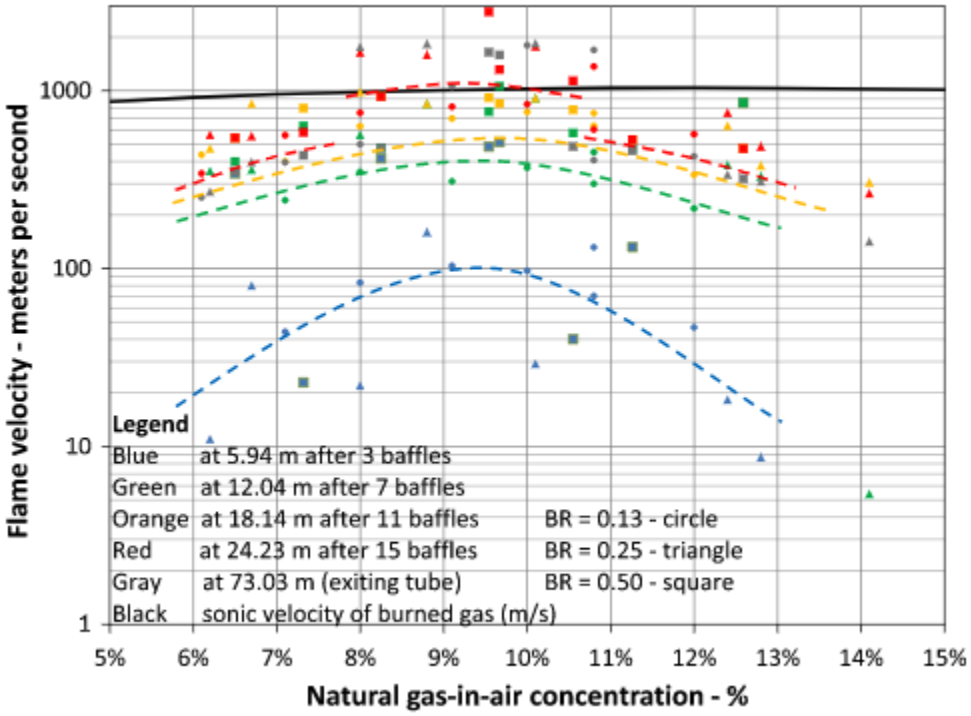

Figure 1.2: GETF flame velocities vs. tube length and natural gas composition. Reprinted from [2, 3]

At the GETF Gamezo et al. [3] analyzed the detonatability limits of methane-air mixtures. They showed detonation limits of 5.3%(lean) and 15.6%(rich) noting that additional fuel impurities would increase the detonability of the mixture. This is attributed to the decrease in ignition delays from additives like ethane, propane or higher alkanes. The decreased ignition delays lead to a shorter ZND induction length, the distance from the leading shock to the maximum thermal gradient in the ZND profile. The addition of 8% ethane in natural gas would decrease the induction length by a factor of 2. Due to the variance in natural-gas composition, there is uncertainty in the explosive properties of natural-gas mixtures. These properties can vary significantly from that of pure methane-air compositions.

GETF test #	NG-air (%)	BR	X_{ru}	X_{DDT}
106	8.00	0.25	21	22.5
100	8.25	0.50	21	22.5
105	8.80	0.25	18	18
127	9.10	0.13	22.5	22.5
95	9.54	0.50	18	18
96	9.67	0.50	18	21
117	10.00	0.13	18	21
104	10.10	0.25	12	18
98	10.55	0.50	15	18
116	10.80	0.13	18	22.5

Table 1.2: Summary of GETF DDT measurements. Reprinted from [2, 3]

Kessler et. al [16] numerically investigated flame acceleration and DDT in stoichiometric methane-air systems in long channel configurations with obstacles. The channel diameters considered were 7.6cm, 17.4cm, and 52cm. An achievement was to develop simplified models for chemical reactions that could be used for both laminar flames and detonations. They found minor differences in flame acceleration for 10-15% variations in laminar flame speed. Kessler found the distance to DDT more sensitive to chemical model parameters. The exact prediction of the location of DDT is extremely difficult and dependent on system geometry and thermodynamic conditions. For methane-air mixtures, they computed detonation cell size λ=$13-31cm$ and correlated the ratio of λ/x_d=$43-87$.

1.2.2 Effect of Fuel Mixtures

Only recently have gas-phase fuel blends been investigated, with significant studies on hydrogen-alkane blends having been performed. This is primarily motivated by the inherent danger with current hydrogen based technologies. These studies have shown large impacts on the explosive behavior of hydrogen mixtures with alkane additives. Heavier hydrocarbon additives in hydrogen have strong stabilizing effects due to the increase in activation energy and autoignition delay times

in the fuel blends[25, 26]. Small amounts of inhibitors (e.g. propane or methane) to hydrogen can decrease the detonability of the mixture, related to detonation cell size (λ) where the detonation properties of such mixtures where governed by the heavier fuels [25, 27]. Methane, ethylene, and propane were all capable of significantly reducing the temperature and burning velocities of hydrogen-air flames [26]. Sorin et al. [28] obtained a series of data for detonation cell size (λ) and DDT transition length (L_{DDT}) which showed a correlation of $L_{DDT} = 40 - 50\lambda$. Zhang et al. [29] measured detonation cell size with lighter hydrocarbons in methane-hydrogen-oxygen mixtures and found a linear relationship for detonation cell size by scaling by the ZND induction zone length (Δ_I): $\lambda = 34.62\Delta_I$. Cheng et al. [27] calculated induction length for the same hydrogen-alkane blends and determined the ratio of induction length to cell size ranges from 35 to 45. Thus, the addition of methane into hydrogen mixtures increased induction length, cell size, and L_{DDT} accordingly. These studies all included blends of high reactive fuels (hydrogen) with relatively low reactive fuels (methane and propane). It is unclear if these relationships still hold for fuel blends with similar reactivity and activation energy.

For alkane-alkane blends, few studies exist with respect to DDT, primarily focusing on more fundamental aspects and autoignition behavior. These fundamental experimental studies performed with shock tubes and rapid compression machines, have shown a few percentage of higher-hydrocarbon to significantly promote the ignition of methane-based fuels [30, 31]. The autoignition delay times fit the Arrhenius model of the form

$$\tau_{ign} = A_f \left[\mathrm{CH_4}\right]^{a1} \left[\mathrm{C}_x\mathrm{H}_y\right]^{a2} \left[\mathrm{O_2}\right]^{b} e^{(E_a/RT)} \tag{1.1}$$

Where A is an empirical constant, E_a is the effective global activation energy, $[\mathrm{CH_4}]$ and $[\mathrm{O_2}]$ are the molar concentrations of the fuel and oxygen respectively. R is the universal gas constant and T is the initial mixture temperature in Kelvin. The results show a dramatic decrease (30-50%) reduction in autoignition times with the addition of 5%-10% ethane or propane in methane based fuel [31]. Further addition of impurity continued to reduce delay, but not as dramatically. These

studies show that natural gas ignition chemistry can be suitably represented by methane-ethane or methane-propane mixtures [32].

Crane et al. [33] studied detonation behavior difference in methane, ozonated methane, and natural gas, noting that all mixtures were qualitatively identical except in induction length. The mixtures, selected by Monte Carlo sampling, showed a narrow band in detonation behavior due to natural gas composition. Ozoneated methane and natural gas had significantly (50%) shorter induction lengths which lead to more predictable detonation behavior. Natural gas extends the detonation limits making it a more preferable fuel for detonation based engines compared to methane. This study, however did not investigate flame acceleration and DDT, only focusing on propagating detonation waves.

In summary, DDT is now a well-studied phenomena with supporting theories on the evolution from flame acceleration to propagating detonation. Experimental work has been performed on natural-gas systems, but most computational work has focused on hydrogen or methane as a reactive gas. For fuel blends, most studies have focused on the use of heavier hydrocarbons for stabilizing hydrogen detonation. To this authors knowledge, the effects of heavy hydrocarbon impurities present in natural-gas, such as propane and ethane, have only been studied from a fundamental standpoint. There is little to no data or insight available on the difference in flame acceleration, detonation and DDT in pure methane and realistic natural gas mixtures.

1.3 Relevance

The prevention of DDT in confined spaces is a daunting task. Understanding the conditions which promote the transition from deflagration to detonation can help make progress to this goal. Knowing where DDT occurs helps engineers construct designs that are safe. If detonation were to occur, critical safety mechanisms should be placed well downstream to reduce excess overpressure created near DDT. Such mechanisms should be well capable of handling detonation temperature and pressures. Understanding these explosions is important for safety science and practical applications. This risk is shared by all industries which confine reactive gases, potentially leading to DDT. In aerospace applications and detonation-based propulsion systems, knowing where DDT

occurs helps optimize designs. Weight is kept to a minimum for performance and understanding where to strengthen components is critical to maintaining system integrity in the case of an accidental explosion. In the chemical process and refining industries, reactive gases are transported and processed in pipelines and reactors. For cost effective reasons, industrial piping is often only designed to withstand moderate overpressures. Protection through explosions venting devices often is only effective against deflagrations. Detonation in such scenarios is often catastrophic. This research aims to answer the following questions: What role do impurities such as propane and ethane impurities play in the DDT process? Does the presence of impurities effect the flame acceleration of fuel-air mixtures? Does the inclusion of these impurities effect the length it takes for DDT to occur from ignition? What effect do heavy hydrocarbon impurities have on the propagation and extinction of detonation waves?

2. RESEARCH METHODS*

Numerical simulation now provides a pivotal role in the investigation of reacting flows. Simulations give insight to mitigate risk and provide key understanding into experimental efforts. This is not to say that numerical simulation should replace experimentation for investigating reactive flows and DDT, however they should augment and inform future experimental efforts. This section details the methods and models used in the following study.

2.1 Numerical Model

The numerical simulations solve the two-dimensional (2D) fully-compressible reactive Navier-Stokes equations for conservation of mass, momentum, energy and species. The reactants are perfectly mixed and are assumed to behave as an ideal gas.

$$\frac{\partial \rho}{\partial t} + \nabla \cdot (\rho \vec{u}) = 0 \tag{2.1}$$

$$\frac{\partial \rho \vec{u}}{\partial t} + \nabla \cdot (\rho \vec{u} \vec{u}) + \nabla p = \nabla \cdot \tilde{\tau} \tag{2.2}$$

$$\frac{\partial (\rho E)}{\partial t} + \nabla \cdot ((\rho E + p)\vec{u}) = \nabla \cdot (\vec{u} \cdot \tilde{\tau}) + \nabla \cdot (\kappa \nabla T) - \rho q \dot{\omega} \tag{2.3}$$

$$\frac{\partial (\rho Y)}{\partial t} + \nabla \cdot (\rho T \vec{u}) = \nabla \cdot (\rho D \nabla Y) + \rho \dot{\omega} \tag{2.4}$$

$$p = \rho R T / M \tag{2.5}$$

*Parts of this section is reprinted from "Numerical simulation of methane-air DDT in channels containing trace amounts of impurities" with permission from Kunka, L.N., Proceedings of the Mary Kay O'Connor Process Safety Symposium, College Station, TX, 2020, and from "Numerical simulations of flame acceleration and DDT in natural gas: the effects of trace propane and ethane" with permission from Kunka, L.N., 2020 American Physical Society Division of Fluid Dynamics, Chicago, IL, 2020.

$$\tilde{\tau} = \rho\nu((\nabla\vec{u}) - (\nabla\vec{u})^T - \frac{2}{3}(\nabla\cdot\vec{u})I) \tag{2.6}$$

$$E = \frac{P}{(\gamma-1)\rho} + \frac{1}{2}(\vec{u}\cdot\vec{u}) \tag{2.7}$$

where ρ is the density, t is the time, p is the pressure, $\vec{u}$ is the velocity vector, T is the temperature, E_a is the specific total energy, Y is the mass fraction, q is the chemical energy release, $\dot{\omega}$ is the chemical reaction rate, κ is the thermal conductivity, D is the mass diffusivity, R is the universal gas constant, M is the molecular weight, γ is the specific heat ratio, ν is the kinematic viscosity, $\tilde{\tau}$ is the viscous stress tensor, I is the unit tensor, and where the superscript T denotes a matrix transposition.

The diffusion properties of the mixture are temperature depended and defined as

$$K = \kappa_0 c_p T^{0.7},\ D = D_0 T^{0.7}/\rho,\ \nu = \nu_0 T^{0.7}/\rho \tag{2.8}$$

The reaction rate ($\dot{\omega}$) represents the combustion process where fuel and oxidizer is converted to product, releasing energy in the process, the definition of which closes the set of equations. Section 2.2 details the implementation of the reaction mechanisms into the numerical solver.

2.2 Reaction Modeling

Reacting flows equations in Equation 2.1-2.7 deviate from the traditional Navier-Stokes through the implementation of source terms in the energy equation. These source terms represent the chemical reactions taking place in the fluid. Ultimately these source terms should describe when, where, and at what rate reactions are to take place as well as prescribe the appropriate amount of heat release for all phases of the reaction.

Combustion modeling for reacting flows is an extremely vast field. A plethora of models have been developed to accurately represent the reaction of a mixture. The advantages and disadvantages of the various modeling approaches are indicated by the quantitative and qualitative comparison of the model predictions with experimental data. In general, the complexity fo the chemical kinetics model used decreases as the complexity of the flow increases. A summary of chemical kinetics models used in complex flows is summarized in [34].

Reactions can be generally assumed to take a fuel and oxidizer at an equivalence ratio (ϕ) to its combustion products releasing heat in the process. In a numerical simulation, each cell can be considered an individual reaction taking its contents from state 1 to state 2 after a time step dt. When using a split time update, the source terms are updated separately from any flux updates. Thus the hydrodynamic operators will not influence the reaction step. The general formulation for the combustion process is summarized below.

$$Fuel + Oxidizer \rightarrow Product + Heat \quad \text{and} \quad \phi = \frac{fuel/oxidizer}{fuel/oxidizer}_{stoichiometric}$$

2.2.1 One-Parameter Chemistry Models

The most simplistic chemistry model require only one parameter to locally describe the combustion process. Such examples include the adiabatic equilibrium and laminar flamelet models. These one parameter models rely on the underlying assumption that the reaction proceeds at a rate much faster than the rates of any fluid processes. The fluid properties are at each location are the thermodynamic equilibrium values of the local value of the mixture fraction, often the local fuel-air ratio for flames. The main advantage of one-parameter models is the simplicity. Due to this, they have been extensively used in the simulation of turbulent reacting flows.

These model works well for hydrogen-air flames even at low Reynolds number, corresponding to slow mixing rates. For methane-air flames however, this agreement between model predictions and experimental data is poor as the assumption of fast chemical time-scales compared to mixing/turbulent time-scales begins to fail. Due to the relatively slow reaction rates of methane-air

mixtures, a more detailed chemical kinetics model is required for natural gas flames.

2.2.2 Global Reaction Model

Two-parameter chemistry models, often called global reaction models, are the next step in adding complexity to the one-parameter models, using a single reaction rate and 3 fluid species (fuel, oxidizer, product). These models are more applicable than one-parameter models as they include a reaction that proceeds as a finite rate. The rate of reaction if often expressed in terms of a progress variable c often defined as

$$c = [products]/[products]_{eq} \quad \text{or} \quad c = \frac{T_b - T}{T_b - T_0} \tag{2.9}$$

Where $[products]$ and $[products]_{eq}$ are the concentration of products locally and at equilibrium respectively. The progress variable c can also be defined through the local temperature with respect to ambient temperature and the adiabatic flame temperature. The progress variable can range from 0 (unreacted) to 1 (complete reaction). The rate of change of the progress variable is of Arrhenius form and a function of reactant concentrations and temperature

$$\frac{dc}{dt} = A[R_1]^a[R_2]^b e^{(-E_a/RT)} \tag{2.10}$$

Where A is the pre-exponential factor and E_a is the overall activation energy. Additionally, a and b are the orders of the reaction with respect to the reactants R_1 and R_2. The parameters needed for the global reaction model are obtained by fitting experimental data or by detailed kinetics. For various hydrocarbon fuels including methane (CH_4), this represents the general reaction,

$$\mathrm{C}_n\mathrm{H}_m + (n + m/4)\mathrm{O}_2 \rightarrow n\mathrm{CO}_2 + m/2\mathrm{H}_2\mathrm{O} \tag{2.11}$$

From gas kinetic theory, the exponential term in the reaction equation 2.10, represents the portion of molecules which have enough energy to undergo chemical reactions. Lowering the temperature, or increasing amount of energy required for reaction (E_a) effectively reduces the

reaction rate. The rate is depended on the molecular concentrations of the reactants and is fitted to experimental data with empirical constants.

Comparison of model calculations and experiential data should be in good agreement, as the experiments where used to derive the global kinetics parameters. Kessler et al. [16] made significant progress in using a single global reaction for methane-air mixtures, particularly in respect to DDT. Additionally, for the simulation of flames at a variety of equivalence ratios, polynomials for reaction parameters as a function of local ϕ can be defined [17].

Global reaction models are not without drawbacks. Kinetic mechanisms based on a single reaction rate of the Arrhenius law cannot recreate both endothermic and exothermic regions of the reaction. For example, fuels undergoing molecular breakdown (dissociation or pyrolysis) or phase change first require energy to break into simpler hydrocarbons. For fuels with relatively small endothermic regions, this model could be applicable. Kessler et al. [16] noted that the one step model described cannot reproduce all properties of flame and detonations exactly, however it can give reasonable approximations of the key length and times scales in the various stages of flame acceleration and DDT. This trade off of physical accuracy with computational efficiency is key to being able to systems of realistic sizes.

2.2.3 Detailed Kinetics

The detailed kinetics approach to combustion modeling aims to model the entire reaction through the elementary reactions of each individual species as well as any intermediate species or radicals that might only exist for a short duration. The rates and associated coefficients at which each species is created and consumed is often determined from experimental data and should be independent of fuel. These rates coupled with an equation of state (EOS) that comes from tabulated values or polynomials created from experimental data. This approach should provide better prediction of the combustion process since, in principle, there are no empirical steps. A general form of an elementary reaction follows as:

$$A + B \leftrightarrow C + D$$

With a forward rate constant and forward reaction rate respectively :

$$k_f = AT^b e^{-E_a/RT} \quad \text{and} \quad R_f = [A]\,[B]\,k_f$$

For reversible reactions, the reverse rates follow suit. Chemical equillibrium is achieved when $R_f = R_b$ for all species. Additionally, various forms of reaction rates including three body reactions, pressure dependent reactions, falloff reactions, etc. These can be fitted to the elementary reaction as dictated by experimental data.

This combination of all species and reaction rates equates to a system of coupled, non-linear ODEs that can be represented by $Ax = b$ where x is the state of the fluid, A is the matrix of reaction rates, and b is the rate of change of the species. This system of ODEs can often be stiff due to the vast difference in rates represented. Detailed kinetics can be solved explicitly or implicilty. Transient species might need a more strict time-step to adequately resolve the reaction.

Reaction	A	b	E_a
OH+CH3<=>CH2+H2O	5.600E+07	1.600	5420.00
OH+CH3<=>CH2(S)+H2O	6.440E+17	-1.340	1417.00
OH+CH4<=>CH3+H2O	1.000E+08	1.600	3120.00
OH+CO<=>H+CO2	4.760E+07	1.228	70.00
OH+HCO<=>H2O+CO	5.000E+13	.000	.00
OH+CH2O<=>HCO+H2O	3.430E+09	1.180	-447.00
OH+CH2OH<=>H2O+CH2O	5.000E+12	.000	.00
OH+CH3O<=>H2O+CH2O	5.000E+12	.000	.00
OH+CH3OH<=>CH2OH+H2O	1.440E+06	2.000	-840.00

Table 2.1: Selected reaction set from GRI 3.0 - Mech[5]

The computational complexity of computing reactions with detailed kinetics requires significant computational resources or simplified simulations. Detailed kinetics require more complex treatments of diffusion fluxes via multicomponent or mixture averaged formulations. In general, the more species included in the mechanism, the more memory per computational cell. The more reactions included, the more compute operations to perform. The inversion of the matrix generally scales with $\mathcal{O}(M^3)$ where M is the number of reactions. For complex chemistry such as realistic fuels or soot formation, this becomes an enormous computational expense. This overhead can be so high as to limit the extent of calculations. It becomes too computationally expensive to compute detailed kinetics of large physical systems. Simply put, the computational cost for detailed kinetics becomes limiting for large-scale multidimensional simulations. This crutch has lead to a significant effort to reduce the complexity of the detailed mechanisms to the minimal subset of species and reactions required to accurately reproduce the physical behavior of the reaction.

Special consideration should be used when determining the applicability of a detail kinetic model. Not all detailed mechanisms are applicable to a wide range of temperatures and pressures, where reactions rates can vary greatly. Particularly for DDT and detonations these mechanism can fail to reproduce experimental results due to the large pressure increase.

2.2.4 Tuned Chemical Diffusion Model

For simulating realistic scenarios and systems for DDT with full detailed chemical models is computationally prohibitive. Additionally, the detailed models are usually inaccurate for high-temperature, high-pressure environments in which DDT occurs. In favor of computational efficiency, the tuned chemical diffusion model (CDM) builds on the global reaction model with help from detailed kinetics. Combustion and the conversion of fuel to product is modeled using a calibrated single-step chemical-diffusion model (CDM) where the reaction rate ($\dot{\omega}$) is defined as

$$\dot{\omega} = \frac{dY}{dt} = -A\rho Y exp(-\frac{E_a}{RT}) \tag{2.12}$$

where Y is the fuel mass fraction, t is time, A is the pre-exponential factor, ρ is the fluid density,

E_a is the activation energy, R is the universal gas constant, and T is the fluid temperature.

The selection of the parameters for mixtures which existing data is not available can inhibit the use of global reaction models. The tuned CDM approach aims to remedy this problem[4]. It treats the reaction scheme as an inverse problem. Instead of trying to replicate the reaction rate, the tuned CDM starts with the dynamic behavior of the chemically reacting system and recreates the parameters needed to achieve similar dynamic behavior [4]. I.e. we create a fictitious gas that recreates computational and experimental measurements of its dynamic behavior in a reaction-diffusion system.

In a reacting system the dynamic behavior is the laminar flame and detonation dynamics where the quantities of interest are the laminar flame speed (S_L), the adiabatic flame temperature (T_b), laminar flame thickness (x_{ft}), constant volume flame temperature (T_{cv}), detonation wave velocity (D_{CJ}), and detonation half-reaction thickness (x_d). These quantities are derived from one dimensional laminar flames and ZND detonation using detailed kinetics and are discussed in more detail in Section 3. We match these to the selection of fluid parameters γ, A, E_a, q, κ_0, and M_w.

The selection of these fluid parameters are non-trivial. To generate these CDMs a genetic algorithm and optimization approach is used to find the optimal value for model parameters (γ, A, E_a, q, κ_0, M_w) such that calculated flame and detonation behavior (T_b, T_cv, S_l, x_{ft}, D_{CJ}, x_d) match their specified target values [4]. The target values are those obtained using detailed kinetics through Cantera [35]. The method assess the fitness of each set in the generation, exchanging and mutation the properties of the fittest parent values to then be inherited by the next generation. This model has extensively tested in laminar and turbulent flames, detonations, and DDT [23, 36, 16].

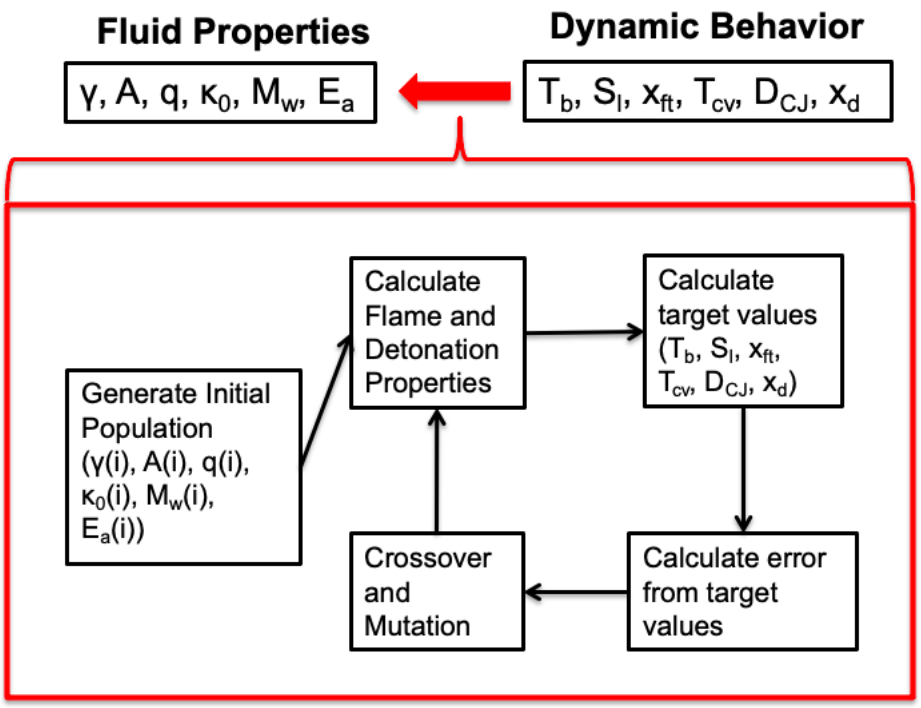

Figure 2.1: Genetic algorithm for creating Chemical-Diffusion Models [4]

This method has various advantages over detailed kinetics. It is computationally and memory efficient allowing for the use on large-scale systems. Using detailed kinetics to optimize and calibrate the tuned CDM allows for simplified global reaction combustion model to close the gap in accuracy and account for experimental measurements. This reduced model can additionally be tailored for different regimes of flame acceleration and detonation. The process makes the simulation of complex reacting flows often present in large-scale practical applications, such as aerospace propulsion and industrial accidents, computationally tractable.

2.3 Reaction Models for Natural Gas

For the simulation of realistic natural-gas DDT and determining the impact of trace impurities, we use detailed kinetics to tune our CDM. Cantera [35] and the GRI 3.0 mechanism [5] were used to determine the laminar flame and detonation behavior of the mixture, then the CDM optimization process was applied for a global reaction rate. The GRI-Mech 3.0 is an optimized mechanism for

modeling natural gas combustion and has been extensively used and tested in literature [5]. The mixtures of interest include stoichiometric methane-air and stoichiometric methane-air with either ethane or propane impurity. We considered impurity concentrations of 1%, 2%, 4%, 6%, 8%. For each impurity, the appropriate percentage of methane in stoichiometric methane-air was replaced with the same percentage of impurity. The tuned global reaction model is then input into the numerical solver detailed in the following section.

	CH_4	C_2H_6	O_2	N_2
1% ethane	0.99	0.01	2.0	7.52
2% ethane	0.98	0.02	2.0	7.52
4% ethane	0.96	0.04	2.0	7.52
6% ethane	0.94	0.06	2.0	7.52
8% ethane	0.92	0.08	2.0	7.52

Table 2.2: Molar composition of ethane mixtures

	CH_4	C_3H_8	O_2	N_2
1% propane	0.99	0.01	2.0	7.52
2% propane	0.98	0.02	2.0	7.52
4% propane	0.96	0.04	2.0	7.52
6% propane	0.94	0.06	2.0	7.52
8% propane	0.92	0.08	2.0	7.52

Table 2.3: Molar composition of propane mixtures

The models developed for trace propane and ethane inclusion show good agreement with lam-

inar flame and detonation behavior. Most models show below 1% error with detailed kinetics predictions. Due to the genetic algorithm and optimization procedure, the models are not guaranteed to be deterministic. The exact selection of a model is dependent on the initial guess and can be subject to local optimization procedures. It is possible for two different models to reconstruct the same reaction behavior. Due to this, interpolation between model parameters is not guaranteed to be smooth nor accurate.

	Impurity	γ	$\frac{E_a}{RT}$	$A(cm^3/g-s)$	qM_w/RT	$\kappa_0(g/s-cm-K^{0.7})$	$M_w(g/mole)$
	0%	1.18	79.17	8.76×10^{13}	42.29	6.86×10^{-6}	27.29
Ethane	1%	1.19	81.38	1.26×10^{14}	41.36	6.88×10^{-6}	27.29
	2%	1.19	84.10	1.95×10^{14}	40.39	6.94×10^{-6}	27.35
	4%	1.19	81.59	1.32×10^{14}	40.50	6.90×10^{-6}	27.42
	6%	1.19	78.95	8.82×10^{13}	40.64	6.81×10^{-6}	27.27
	8%	1.19	79.89	1.05×10^{14}	39.92	6.81×10^{-6}	27.30
Propane	1%	1.19	88.65	4.139×10^{14}	39.51	7.009×10^{-6}	27.37
	2%	1.19	82.70	1.573×10^{14}	40.57	7.024×10^{-6}	27.50
	4%	1.19	81.78	1.453×10^{14}	40.20	6.860×10^{-6}	27.11
	6%	1.20	82.54	1.720×10^{14}	39.41	6.881×10^{-6}	27.38
	8%	1.21	91.77	8.225×10^{14}	37.03	6.890×10^{-6}	27.13

Table 2.4: CDM parameters for methane-air with propane or ethane impurity

Ethane CDM and Target Properties

Impurity	$S_l(cm/s)$		$D_{CJ}(m/s)$		$T_b(K)$		$x_{ft}(cm)$		$x_d(cm)$		$T_{cv}(K)$	
	CDM	Target	CDM	Target	CDM	Target	CDM	Target	CDM	Target	CDM	Target
0%	37.7	37.7	1800	1800	2224	2224	0.0446	0.0446	1.68	1.68	2585	2585
1%	37.08	37.95	1806	1805	2229	2228	0.0443	0.0442	1.423	1.423	2588	2589
2%	38.09	38.16	1810	1807	2228	2231	0.0441	0.0439	1.235	1.23	2597	2597
4%	38.56	38.53	1809	1811	2232	2235	0.0434	0.0435	0.9602	0.9596	2602	2600
6%	38.83	38.84	1815	1815	2235	2236	0.0431	0.0431	0.7761	0.7758	2604	2605
8%	39.07	39.05	1817	1818	2233	2234	0.0426	0.0427	0.6475	0.6472	2609	2608

Table 2.5: Comparison of ethane CDM and target values

Propane CDM and Target Properties

Impurity	$S_l(cm/s)$		$D_{CJ}(m/s)$		$x_{ft}(cm)$		$T_b(K)$		$x_d(cm)$		$T_{cv}(K)$	
	CDM	Target	CDM	Target	CDM	Target	CDM	Target	CDM	Target	CDM	Target
0%	37.7	37.7	1800	1800	0.0446	0.0446	2224	2224	1.68	1.68	2585	2585
1%	38.63	38.32	1813	1807	0.0434	0.0438	2225	2237	1.276	1.265	2601	2593
2%	39.03	38.92	1807	1811	0.0435	0.0432	2234	2234	1.056	1.056	2603	2599
4%	39.81	39.76	1822	1817	0.0442	0.0422	2234	2233	0.817	0.817	2606	2607
6%	39.98	40.2	1813	1823	0.0417	0.0414	2225	2222	0.678	0.68	2604	2609
8%	40.17	40.16	1828	1828	0.0409	0.0409	2206	2206	0.591	0.591	2605	2605

Table 2.6: Comparison of propane CDM and target values

2.4 Numerical Solver

The reactive naiver stokes equations outlined in Section 2.1 are solved using the Flame Acceleration Simulation Tool (FAST) [37]. FAST solves the governing equations using a fifth-order-accurate spatial-reconstruction method that includes features from the nonlinear error-controlled WENO scheme [38] and HLLC approximate Riemann solver [39]. The time integration uses a third-order explicit Runge-Kutta scheme. The code includes an immersed boundary algorithm that allows flow computations in and around complicated geometries [40]. Adaptive mesh refinement (AMR) is used to dynamically refine the mesh in areas of interest though the use of BoxLib [17]. AMR helps resolve important flow features such as flames, pressure waves, shocks, and boundary layers.

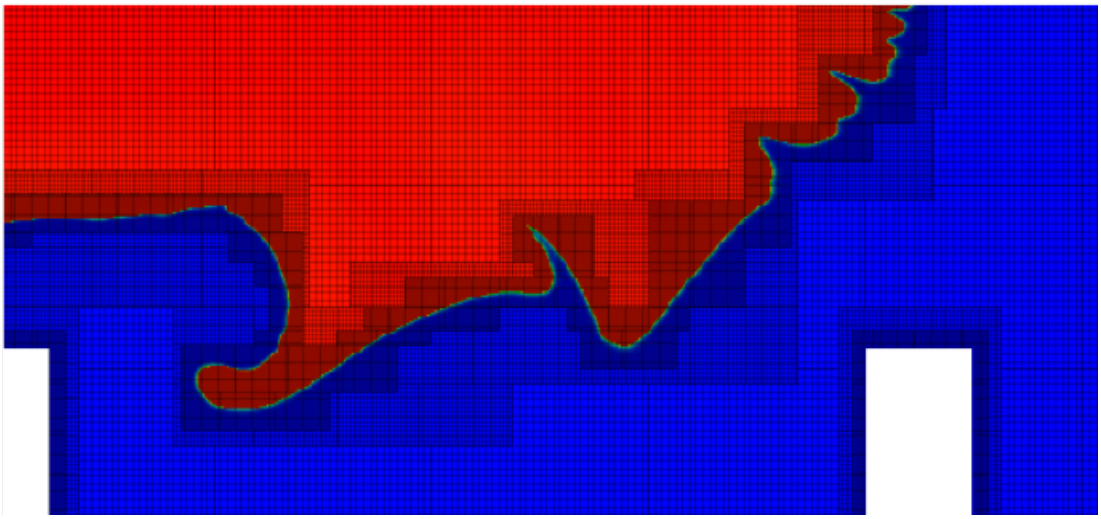

Figure 2.2: Adaptive Mesh Refinement (AMR)

Many numerical investigations are limited by their ability to correctly model and capture physics as well as the assumptions of the underlying models. Current computer hardware limitations restrict the use of detailed physics. Under certain conditions, assumptions about the flow can be made to reduce the complexity of the solver allowing for more computational resources

to focus on the most important flow physics. For example, in turbulence dominated flows, multi-component diffusion models can be abandoned in favor of Fickian or mixture averaged based diffusion models. The effect of diffusion on flame behavior in these turbulence dominated flows is much less that the turbulent mixing due to the advection of the fluid. Additionally FAST does not fully resolve turbulence as would be done in Direct Numerical Simulation (DNS), rather using Implicit Large Eddy Simulations (ILES) to capture the most important turbulent flow features [41].

3. PHYSICS OF REACTING FLOWS*

The process of DDT in channels encompasses several fundamental combustion processes. From the smallest molecular interactions to large scale system response, these effects of these phenomenon cascade both forwards and backwards through the multiscale regimes. In this section, we will analyze each fundamental process as well as coupling of each process to the next. These are useful not only for understanding the dynamic behavior of mixtures in simplified problems, but also as input for the target values for the tuned CDM model. We will start with molecular behavior then discuss one-dimensional laminar flames and detonations. The results presented in this chapter are computed using detailed kinetics and the GRI 3.0 mechanism [5] unless otherwise noted. These and other following simulations are performed under the assumption that the mixture can be modeled as an ideal gas, is in thermal equilibrium, and a Knudsen number small enough to maintain the continuum flow assumption (Kn is the ratio of mean free path to system scale).

3.1 Molecular Scales

At the smallest molecular scales, analysis can quantify two important chemical kinetic behaviors, the amount of heat release during the combustion process and the time scales association with the reaction. This can be achieved through a zero dimension simulation, considering a single cell or parcel of fluid mixture at an initial state and allowing it evolve over time only considering the chemical reactions. In principle, by examining the beginning and final state we can analyze the complete combustion of methane-air mixture

$$\mathrm{C}_n\mathrm{H}_m + (n + m/4)\mathrm{O}_2 \rightarrow n\mathrm{CO}_2 + m/2\mathrm{H}_2\mathrm{O} + \text{heat of combustion} \tag{3.1}$$

The heat of combustion is the negative enthalpy change of the system. The heat of combustion

*Parts of this section is reprinted from "Numerical simulation of methane-air DDT in channels containing trace amounts of impurities" with permission from Kunka, L.N., Proceedings of the Mary Kay O'Connor Process Safety Symposium, College Station, TX, 2020, and from "Numerical simulations of flame acceleration and DDT in natural gas: the effects of trace propane and ethane" with permission from Kunka, L.N., 2020 American Physical Society Division of Fluid Dynamics, Chicago, IL, 2020.

can be calculated by integrating the enthalpies throughout the reaction or over a small step dt. Alternatively for complete combustion, Hess's Law can be used by examining the enthalpy of formation (ΔH_f) of the reactants and products.

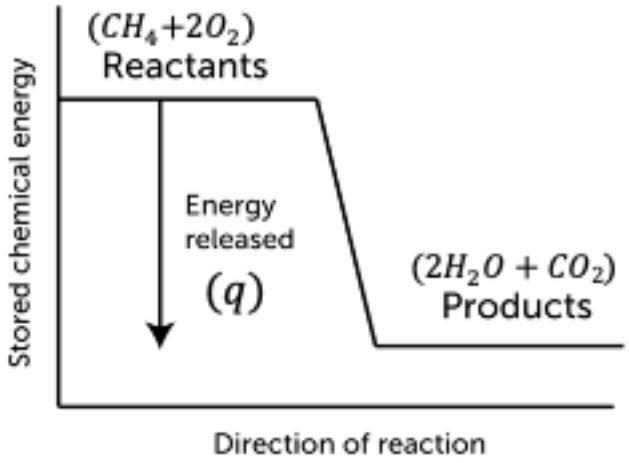

Figure 3.1: Hess's law for methane combustion

$$\Delta H_{rxn} = \sum \Delta H_{f(products)} - \sum \Delta H_{f(reactants)}$$

We can then use $q = \Delta H_{rxn} = c_p \Delta T$ to determine flame temperatures. Adiabatic flame temperature T_b and constant volume flame temperature can then be found using Equation 3.2. Similar analysis can be performed on all methane-impurity blends.

$$T_b = T_0 + \frac{q}{c_p} \quad \text{and} \quad T_{cv} = T_0 + \frac{q}{c_v} \tag{3.2}$$

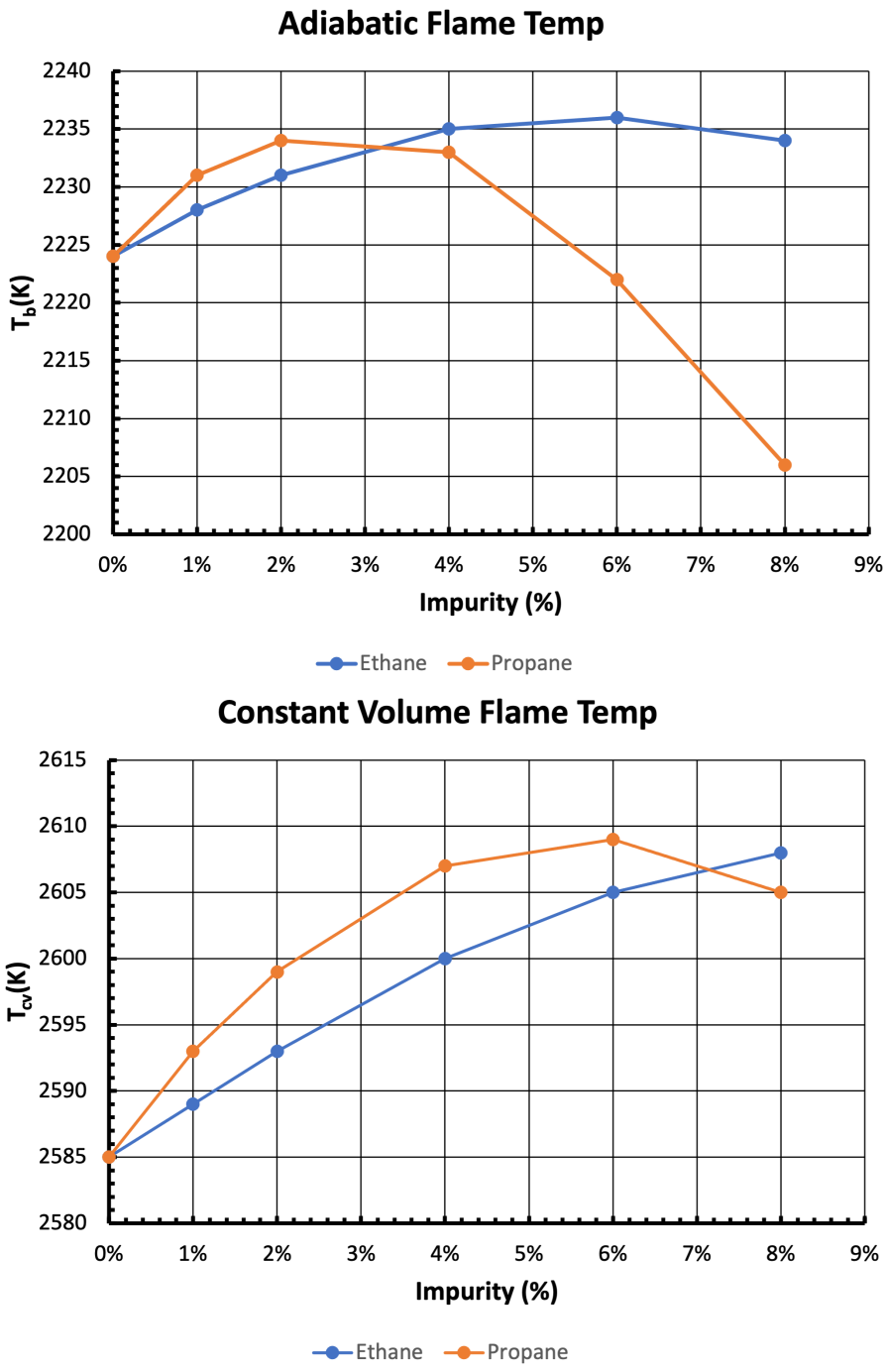

Figure 3.2: (Top) T_b and (Bottom) T_{cv} for trace amounts of propane and ethane

Chemical reactions cannot be assumed to be infinitely fast. Particularly low-reacting compositions such as methane, the reactions proceed at some finite time after exposure to an initial

temperature. If the initial temperature is not above the auto-ignition temperature, no reactions will take place. The auto-ignition temperature for methane, ethane and propane are 868K, 788K, and 743K respectively. Enough energy must be input into the system to start the chain branching reaction. Often for complex hydrocarbon or fuels undergoing phase change (evaporation, pyrolsis, etc.) the reaction can start as an endothermic reaction as the molecules dissociate. The time it takes for the fuel to begin reacting is known as the ignition delay time (τ_{ign}), often measured with time to peak thermicity or maximum OH concentration show in figure 3.3. Ignition delay times for the mixtures of interest are detailed in figures 3.4 and 3.5.

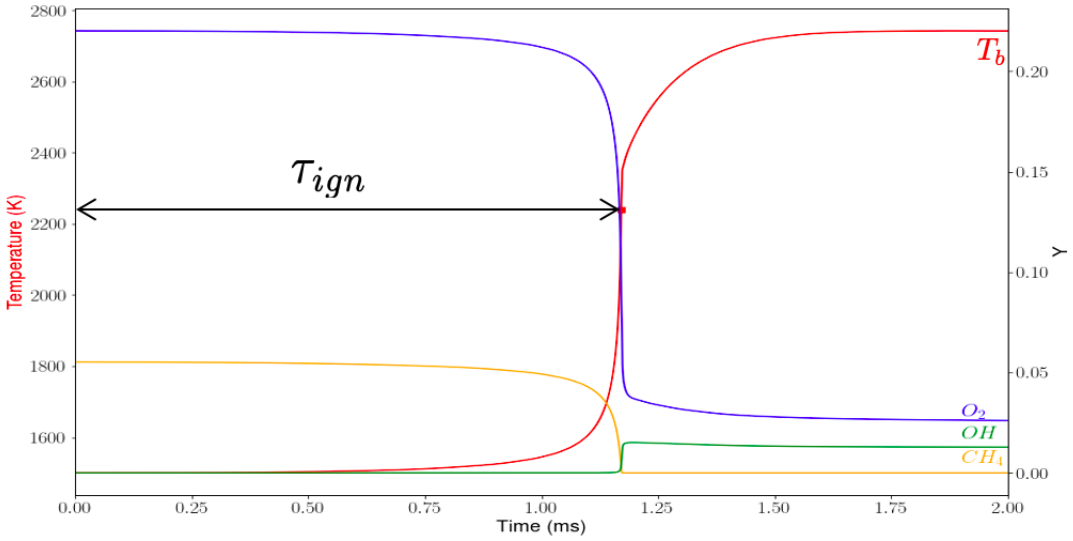

Figure 3.3: Ignition delay for methane-air

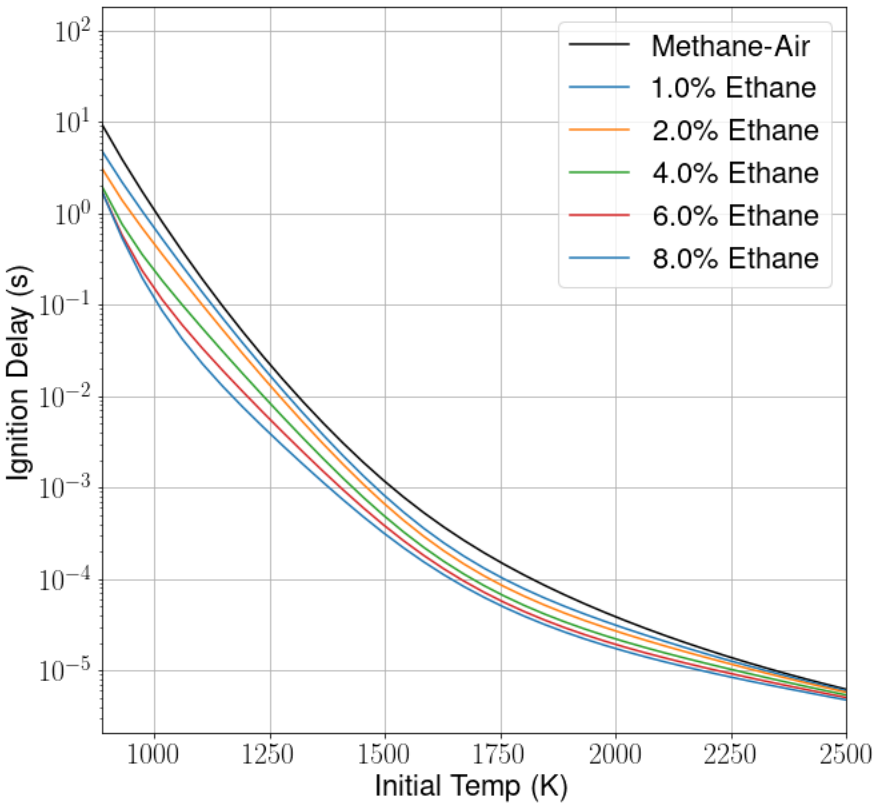

Figure 3.4: Ignition delay for ethane addition

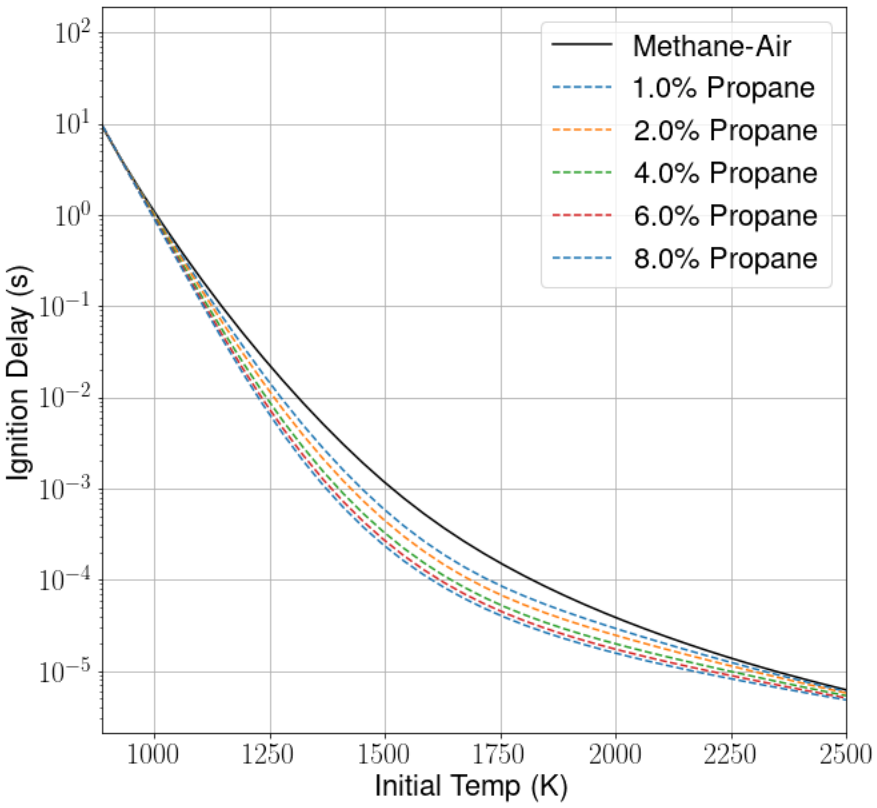

Figure 3.5: Ignition delay for propane addition

We see a large decrease in the ignition delay for the addition of alkane impurity for both propane and ethane at all temperatures. As the initial temperature increases, we see the difference begin to decrease. For low initial temperatures, the time scales are much larger than those relevant in flames and detonations.

3.2 Characteristics of Laminar Flames

By extending the zero-dimensional simulations into one dimensional space, we are able to study the spatial behavior of flows. The one dimensional nature of both laminar flames and detonation waves give insights into multi-dimension behavior and some of the most important parameters required to calibrate a chemical-diffusion model.

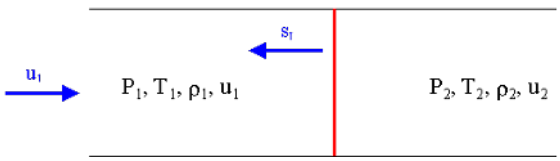

Figure 3.6: Laminar flame setup

Here, we study laminar flames in premixed fuel-oxidizer mixtures. The behaviors will differ from non-premixed systems where the fuel and oxidizer are spatially separated. One useful measurement from 1D simulations is the reaction wave speed called laminar flame speed (S_l) which is a widely used quantifier of the reactive mixture. In one dimension, the reactive Navier-Stokes equations in Equation 2.1-2.7 can be simplified to the steady state form:

$$\frac{d}{dx}(K\frac{dT}{dx}) - \dot{m}c_p\frac{dT}{dx} = -q\rho\dot{\omega} \tag{3.3}$$

Using the boundary conditions $T_{x=-\infty} = T_0$ and $\frac{dT}{dx}|_{x=+\infty} = 0$ where $\dot{m} = \rho_0 S_l$ we can reconstruct the spatial profile.

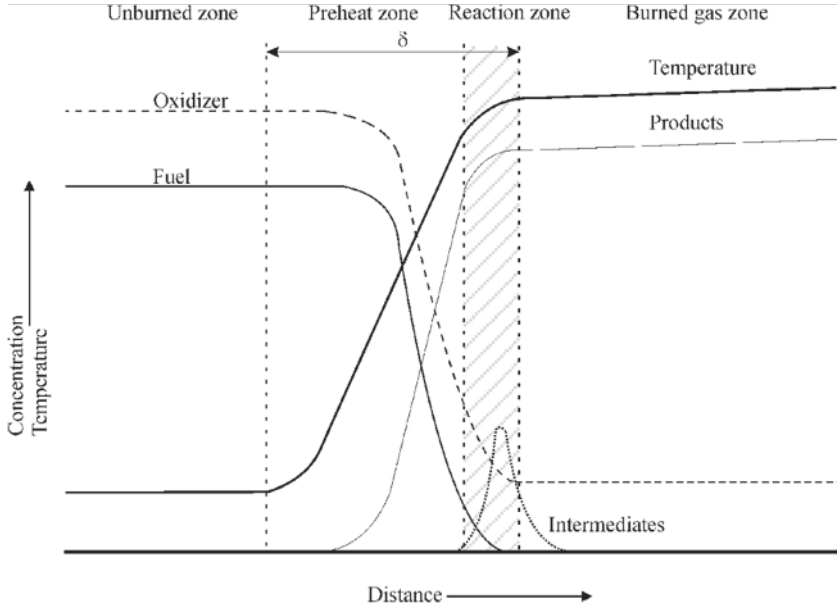

Figure 3.7: Laminar flame profile in stoichiometric methane-air

Integrating over the whole domain determines the adiabatic flame temperature (T_b) and constant volume flame temperature (T_{cv}). This is directly related to the amount of heat release of a given mixture through equation 3.2. This ensures complete combustion where the heat of combustion has been released into the gas.

Using Equation 3.3 and the definition of we can determine a laminar flame speed that satisfies the constrain $T_{x=-\infty} = T_b$. Additionally, from the 1D laminar flame profile we can also determine the laminar flame thickness (x_{ft}) as:

$$x_{ft} = \frac{T_b - T_0}{max|\frac{dT}{dx}|} \tag{3.4}$$

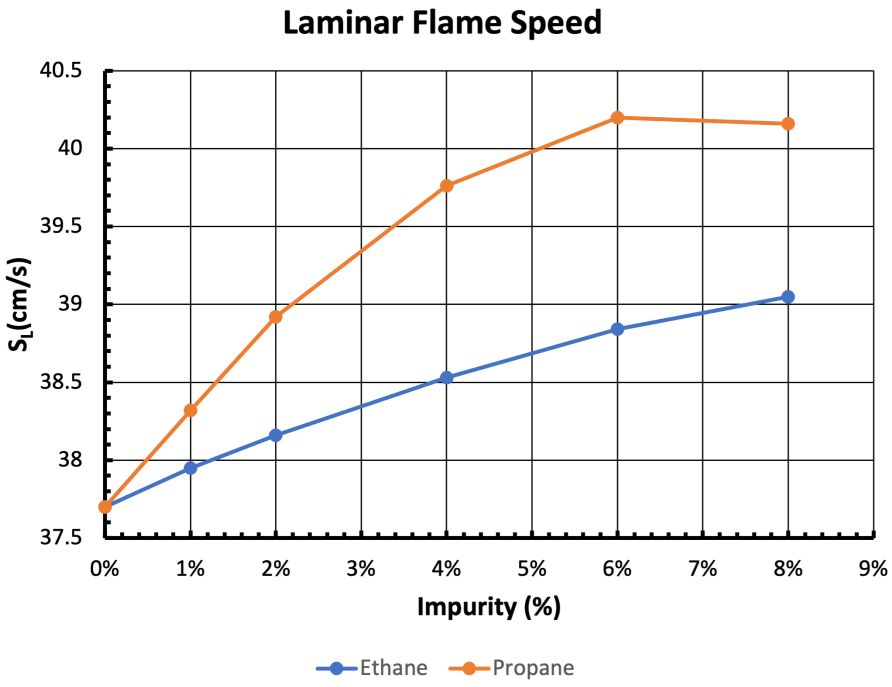

Figure 3.8: S_L for trace amounts of propane and ethane

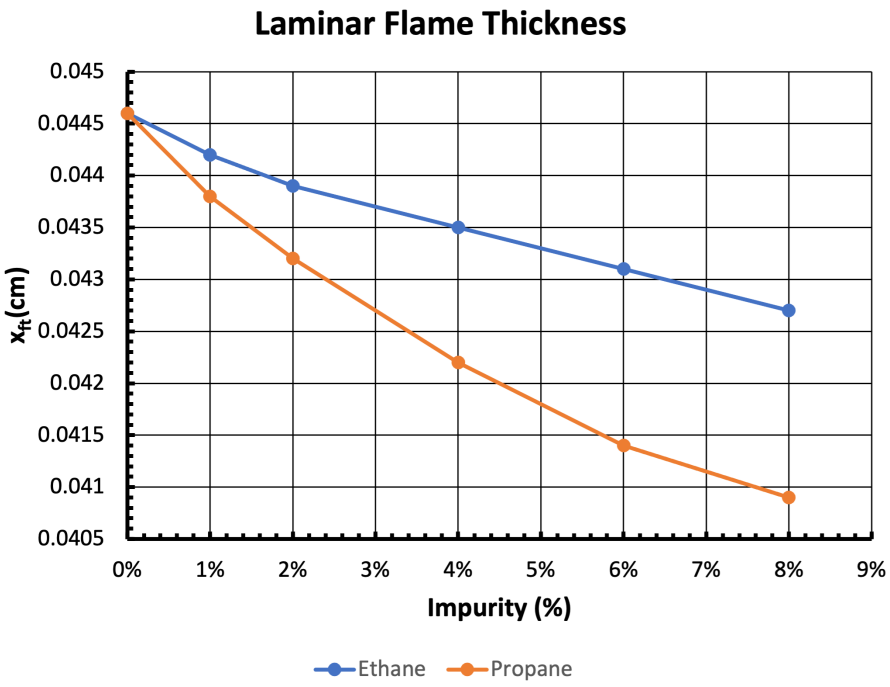

Figure 3.9: x_{ft} for trace amounts of propane and ethane

We see very little change for all fuel mixtures up to the addition of 8% propane or ethane. Particularly for methane-propane blends, we see the effect of impurity on laminar flame speed begin to decline.

3.3 Characteristics of Detonation Waves

Similarly, detonation waves can be studied using one-dimensional analysis. The detonation properties can be computed using the ZND model and Chapman-Jouguet theory. A shock leads the reaction wave at a speed

$$D_{CJ} = c_0 \left(\sqrt{1 + \frac{1}{p_0} \frac{\rho_0(\gamma^2 - 1)}{2\gamma}} + \sqrt{\frac{q}{p_0} \frac{\rho_0(\gamma^2 - 1)}{2\gamma}} \right) \tag{3.5}$$

Starting at the post-shock Von Neumann state (ρ_{vn},p_{vn},e_{vn}) and integrating using Equations 3.6 until you reach the CJ state gives the detonation profile.

$$u = \frac{\rho_0 D_{CJ}}{\rho}, \quad \frac{dx}{dt} = u, \quad \frac{d\rho}{dt} = \frac{q\dot{\omega}\rho(\gamma - 1)}{u^2 - c^2}, \quad \frac{dE}{dt} = \frac{p}{\rho^2}\frac{d\rho}{dt} + q\dot{\omega} \tag{3.6}$$

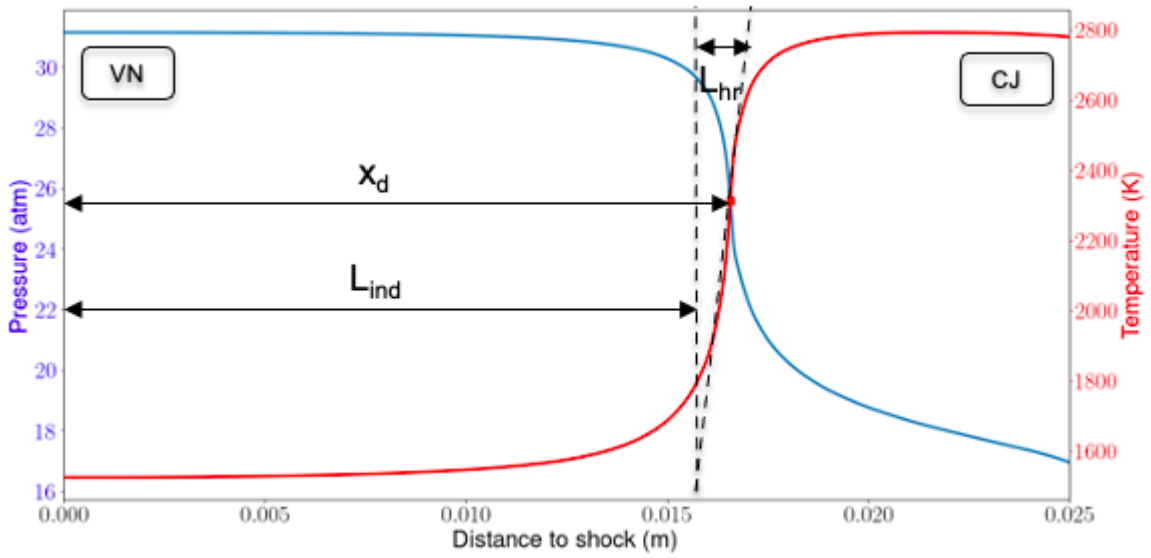

Figure 3.10: ZND detonation profile for methane-air

Using the ZND detonation profile, measuring the distance from the shock to the maximum temperature gradient, we can determine the half reaction length (x_d). The half reaction length is related to the ignition delay approximately by $x_d \approx (D_{CJ} - u_{vn})\tau_{vn}$ where u_{vn} and τ_{vn} are the velocity and igntion delay time at the post-shock Von Neumann state.

Similar to laminar flames, we see little change in the wave velocity (D_{CJ}) for mixtures containing trace propane and ethane. We do see large impact of impurity concentration on x_d. An 8% addition of heavier hydrocarbon reduces the half reaction length by nearly a factor of 3.

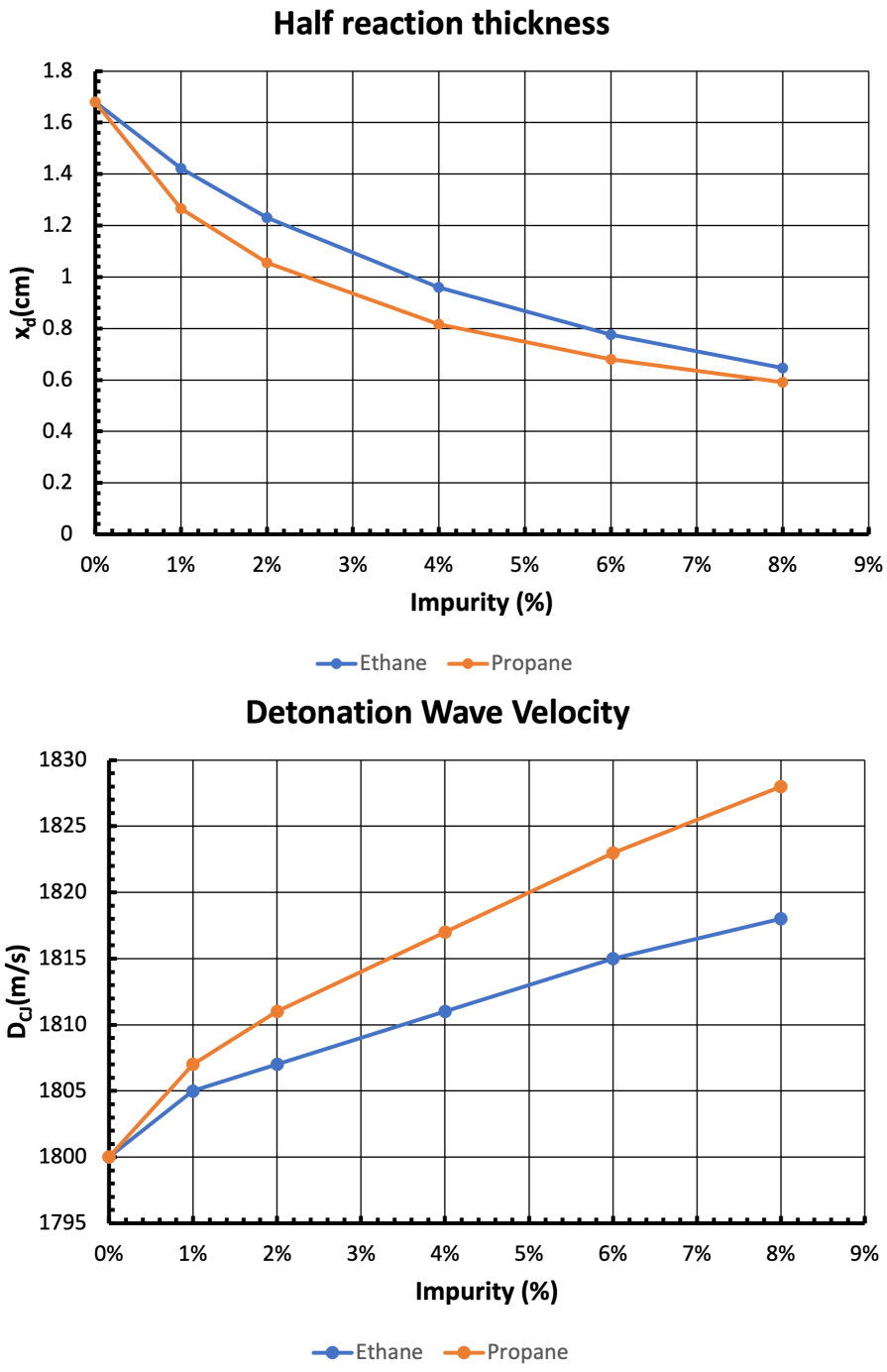

Figure 3.11: (Top) D_{CJ} and (Bottom) x_d for trace amounts of propane and ethane

4. SIMULATION RESULTS*

4.1 Channels with Obstacles

4.1.1 Problem Setup

The computational domain is a long channel with regularly spaced obstacles ($L = D$) with a blockage ratio $br = 0.3$. This configuration is consistent with DDT experiments [42, 2, 20] and is typical for various industrial setting and mines. Previous work has shown effects of blockage ratio, obstacle type and obstacle placement on L_{DDT} [23, 21, 22]. The configurations investigated were $D = 17.4cm$, $D = 52cm$, and $D = 1m$. All geometry ratios were kept constant for each gas mixture. The grid spacing was $dx_{max} = 0.27cm$ and $dx_{min} = 0.03cm$ for all size channels. The flame is initially ignited in the upper left corner with diameter $d_f = 0.25cm$ and allowed to propagate through the channel.

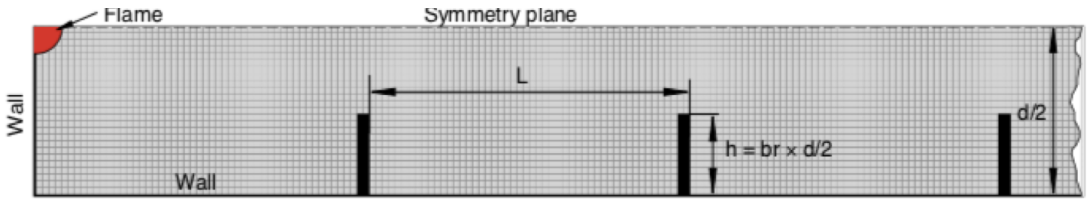

Figure 4.1: Computational domain for channels with periodic obstacles

The upper boundary is a symmetry plane, so we only simulate half the domain. The left and bottom boundaries are walls and the right boundary is open. The obstacles are repeated throughout the length of the channel for as long as required until DDT has been achieved.

*Parts of this section is reprinted from "Numerical simulation of methane-air DDT in channels containing trace amounts of impurities" with permission from Kunka, L.N., Proceedings of the Mary Kay O'Connor Process Safety Symposium, College Station, TX, 2020, and from "Numerical simulations of flame acceleration and DDT in natural gas: the effects of trace propane and ethane" with permission from Kunka, L.N., 2020 American Physical Society Division of Fluid Dynamics, Chicago, IL, 2020.

The simulations presented are studied using two-dimensional geometry, as resolving all relevant scales in three-dimensions would be extremely computationally expensive. Previous work has shown the effects of 2D models on 3D systems. They found that both 2D and 3D simulations show similar trends and mechanisms to DDT, but 3D models have 30-60% shorter distance to DDT. The results combined with experimental data allow us to analyze the common trends among simulations.

4.1.2 DDT Process

The deflagration-to-detonation process seen in the simulations is seen in the figure below and has been previously described in [24, 16, 18]. The following section outlines the steps identified in the DDT process.

4.1.2.1 Laminar Flame Propagation

During the initial stages, the flame ignition propagates into the unburned mixture at the laminar flame speed S_l. In premixed flows, the laminar flame speed is heavily influenced on the thermal conductivity of the mixture and reaction rate. The flame continues to propagate at this laminar flame speed accelerating due to the expansion of the burned medium until the flame begins to interact with the obstacles.

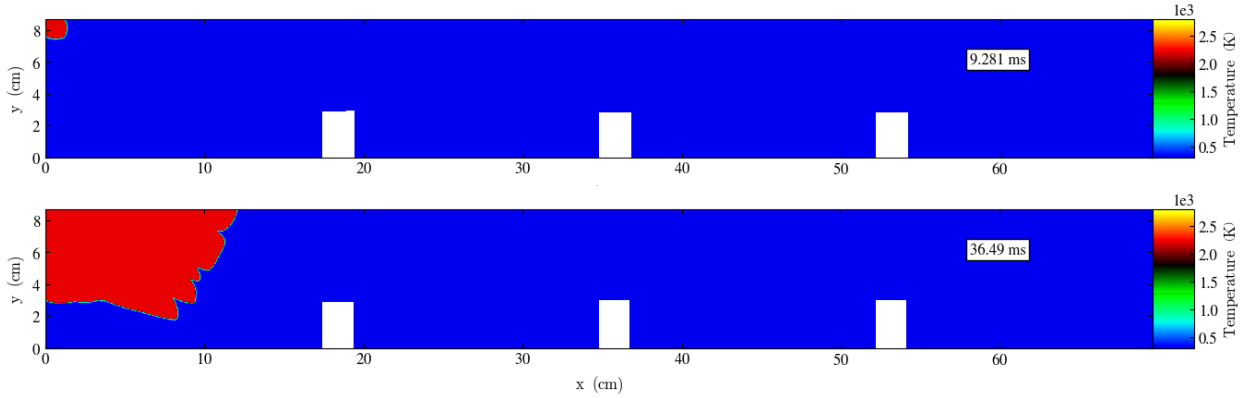

Figure 4.2: (Top) Ignition of flame (Bottom) Flame initially propagating in the channel

4.1.2.2 Flame Acceleration

Flame acceleration occurs primarily due to advection in the gas flow, which can be much greater than laminar and turbulent flame speed. The bulk gas flow is driven by the thermal expansion of the gas behind the flame, which increases with additional heat release from the flame front. The heat release is a function of the flame-surface area, which is increased as the flame is stretched and wrinkling occurs from fluid instabilities and turbulent motion.

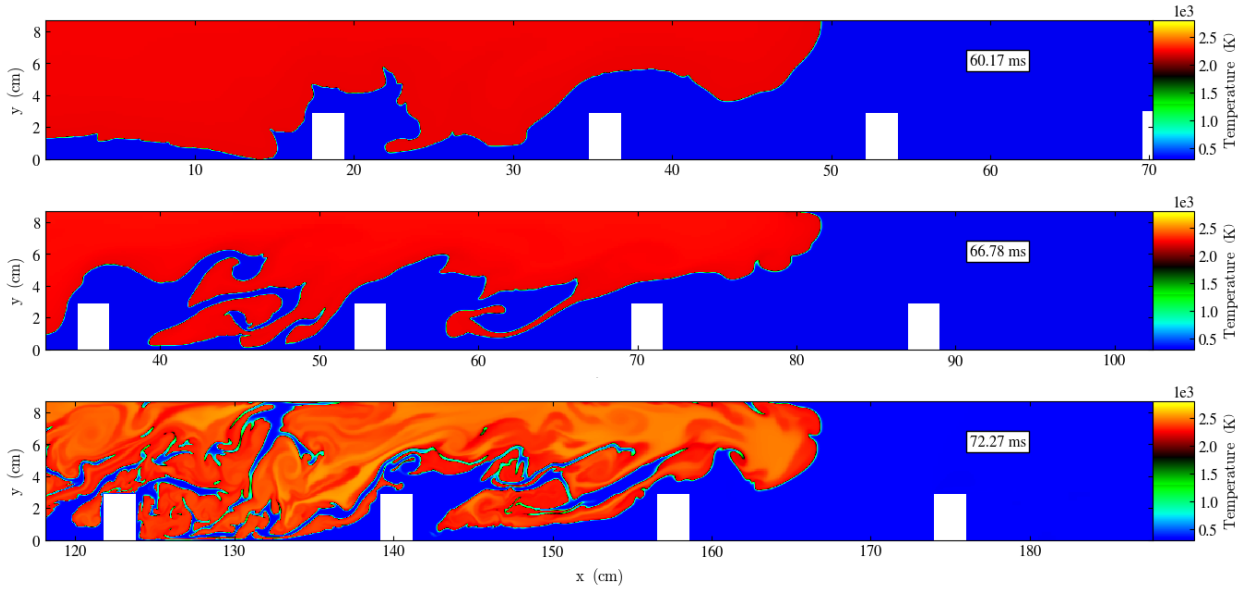

Figure 4.3: Progression of flame acceleration over obstacles

As the flame accelerates, acoustic waves are propagated ahead of the flame front. These acoustic waves can coalesce forming a shock. As the flame approaches the speed of sound, the shock-flame interaction becomes an important mechanism for increased flame acceleration through turbulence generation via Rayleigh-Taylor and Richtmeyer-Meshkov instabilities.

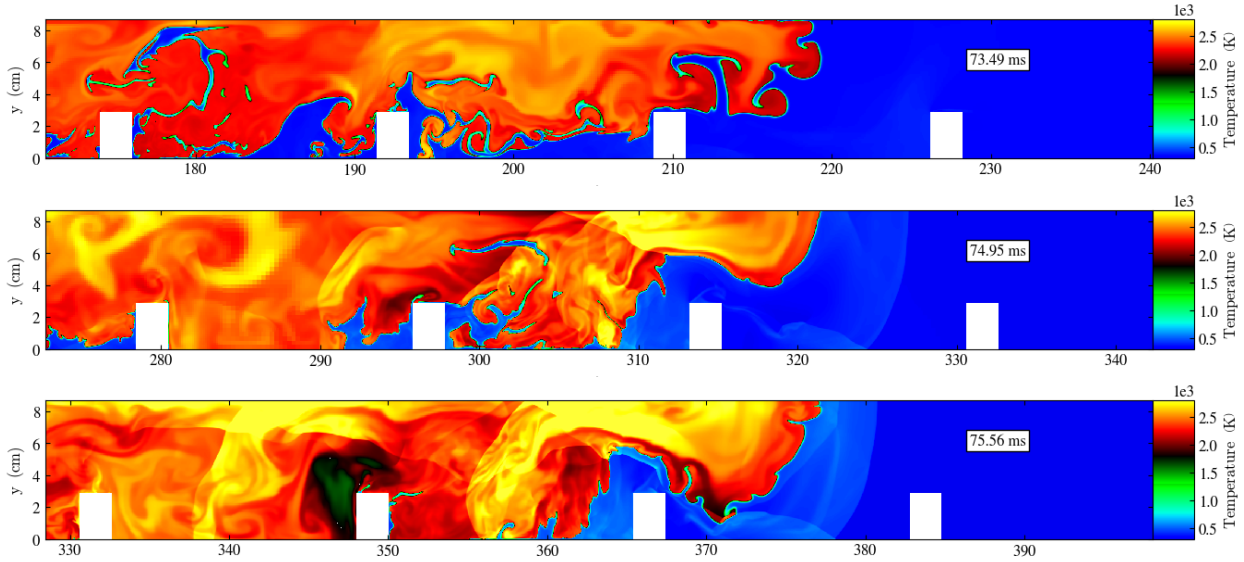

Figure 4.4: Generation of acoustic waves, coalescence, and formation of strong shock

The acoustic wave generated can be better visualized using numerical schlieren to view the density change. The three images above are reproduced below using schlieren. The presence of acoustic waves is shown in the top images, which later coalesces into a strong shock in the following images. In the top image, the acoustic waves can be seen reflecting off the obstacles, causing further turbulence generation and flame acceleration. Additionally, the background flow produces vorticies as it flows past the obstacles.

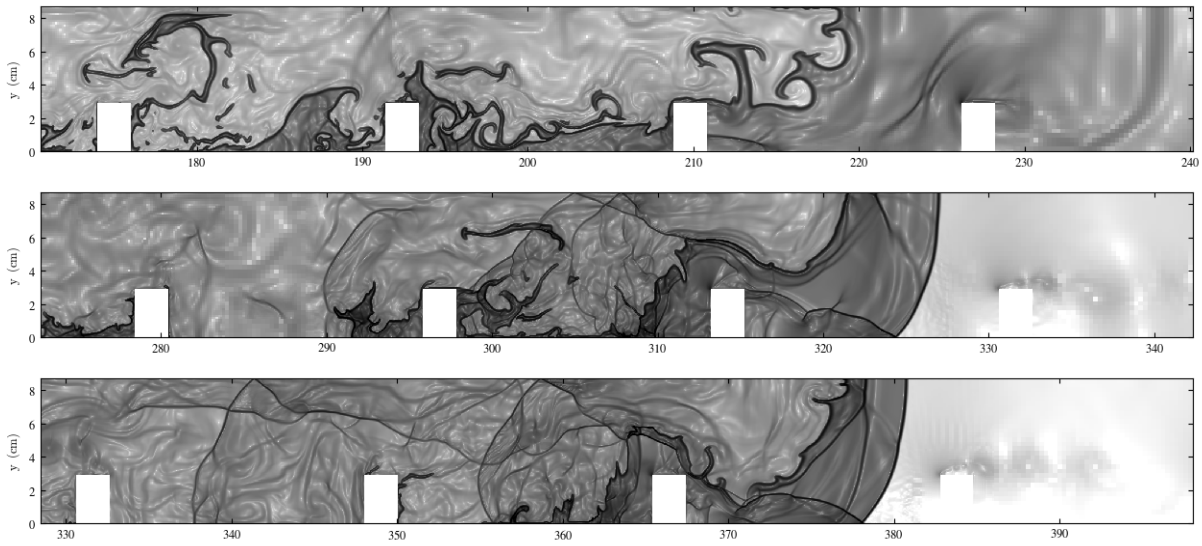

Figure 4.5: Schlieren visualization of acoustic waves and shock formation

During this process of flame acceleration, laminar flame speed (S_l), adiabatic flame temperature (T_b), and speed of sound play a significant role. During this stage of the DDT process the dynamic behavior primarily depends on the initial temperature T_0, the specific heat release q, the ratio of specific heats γ, the pre-exponential factor A, activation energy E_a, and thermal conductivity κ.

4.1.2.3 DDT

The formation of hotspots has been found to be one critical path to DDT onset. Hotspots are created ahead of the flame front in the unreacted mixture. These hotspots have been found in turbulent shock-laden flows such as due to shock reflections, vortices behind mach stems, and multiply shocked regions. We primarily see the formation of hot spot regions in this work due to shock reflections from obstacles in the flow. In Figure 4.6 a hot spot at the base of the obstable at $x = 400cm$ is formed due to the compression from the shock and mach stem.

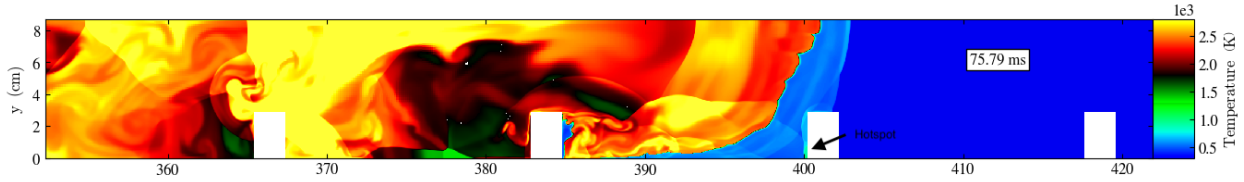

Figure 4.6: Formation of hotspot on obstacles due to shock wave/mach stem

Not all detonation waves from hotspots are guaranteed to survive. DDT can happen many times before a successful detonation wave propagates to the unburned mixture ahead of the flame. In the figure below, the top two cases were not successful in fully transitioning due to entrapment from the preceding flame.

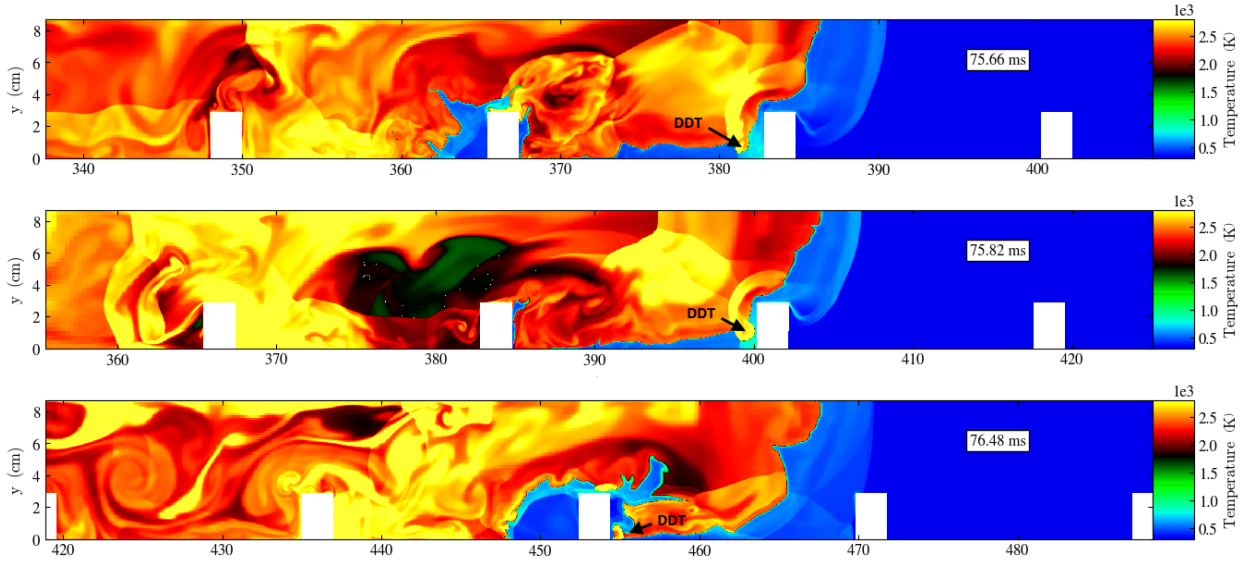

Figure 4.7: (Top) DDT fail (Middle) DDT fail (Bottom) DDT success

The initiation of the detonation from localized hotspot is governed by the Zeldovich gradient mechanism [43]. In these regions, the temperature can be high enough to ignite the unburned mixture. A spatial temperature gradient causes the ignition to propagate as a reaction wave [43] that

can form a strong shock and eventually a detonation. This mechanism to DDT is not guaranteed to survive, and the survival of the resulting detonation wave is dependent on local thermodynamic condition and geometric configuration.

Liberman et al. [44] details the behavior of these hotspots on the success of DDT. The hotspot must be of sufficient temperature as to be above the autoignition temperature and of correct temperature gradient. This temperature gradient creates a non-uniform distribution of induction times, where ignition will occur at the spot with the minimum induction time. The behavior of DDT is influenced by ignition delays behind shocks as well as the behavior of detonation waves. The induction time of a mixture is shown to be an important metric for the investigation of DDT.

$$U_{sp} = |(d\tau_{ind}/dx)|^{-1} = |(\partial\tau_{ind}/\partial T)^{-1}(\partial T/\partial x)^{-1}| \tag{4.1}$$

The value of this wave speed is dependent on only the temperature gradient and $\partial\tau_{ind}/\partial T$. Very steep gradients will decrease the wave speed resulting in the deflagration mode of combustion. Such a steep gradient could be the result of hot walls in the fluid or ignition sources. A zero gradient or uniform thermal distribution above the auto ignition temperature would result in a uniform thermal ignition.

By differentiating the ignition delay curve in Section 3.1 with respect to temperature, we can analyze the effect of impurity on DDT via thermal gradients. The decrease $\partial\tau_{ind}/\partial T$ for impurity addition suggests a decrease in the thermal gradient $\partial T/\partial x$ and in turn hotspot size required for DDT. The change in gradients for temperatures greater than 1000K is small, thus producing minimal effect on wave speed. The impact this effect has on large simulations is likely to be minimal in comparison to hydrodynamic effects.

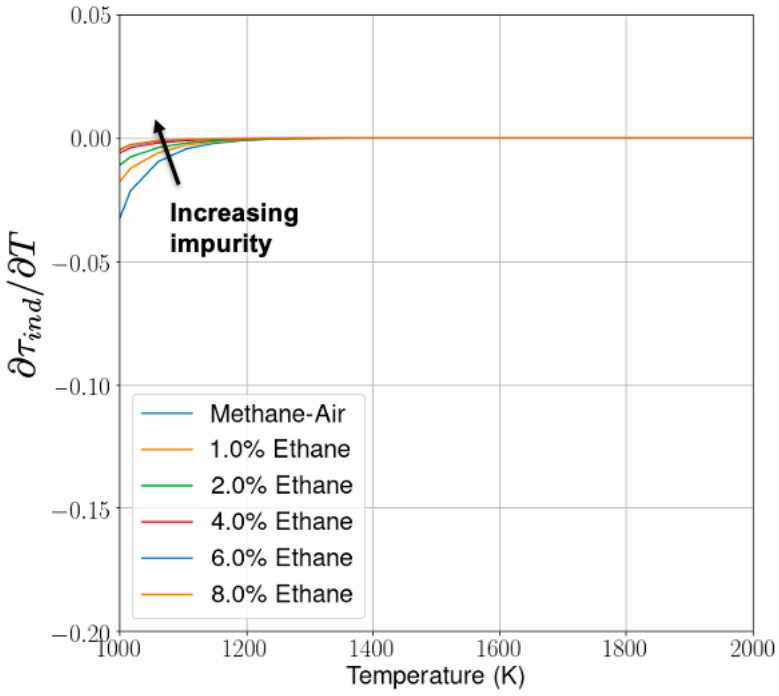

Figure 4.8: $d\tau/dt$ for ethane impurity addition

4.1.2.4 Propagating Detonation Wave

If the resulting detonation survives from DDT, a reaction wave will propagate into any unburned mixture at the Chapman-Jouguet (CJ) speed D_{CJ}. Propagating detonation waves have been extensively studied and are presented in CJ and ZND theory.

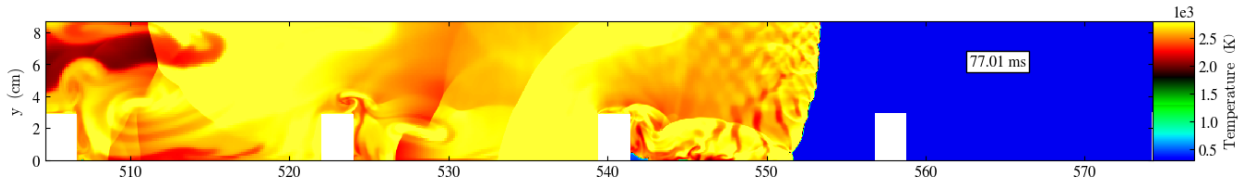

Figure 4.9: Detonation wave after DDT

After DDT, the detonation wave can proceed as a quasi-detonation wave which will often ex-

tinguish as refracts over an obstacle. The wave will then undergo DDT at a hotspot created later in the flow.

4.1.3 Methane-Air DDT

Flame speed is tracked as a function of position and time as it propagates down the channel. Detonation initiation starts when the flame velocity reaches the Chapman-Jouguet velocity D_{CJ} which is approximately 1800 m/s for methane-air mixtures. The detonation wave will overshoot this steady-state velocity as it is overdriven, before settling at the D_{CJ} velocity. Additionally, we can track flame speed as a function of simulations time. Flame velocities and time for methane-air are tracked in fig. 4.10

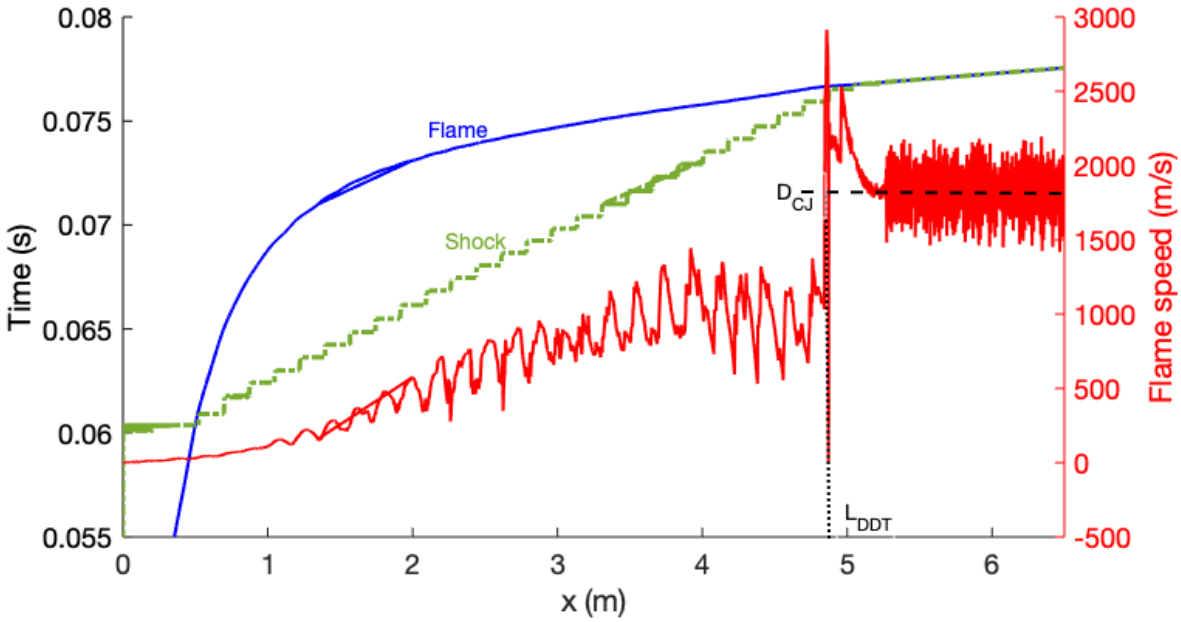

Figure 4.10: Simulation diagnostic for methane-air DDT

Tracking both the flame and leading shock as a propagates down the channel, we can determine DDT onset as the location where the flame velocity has first reached D_{CJ}. We denote this point as L_{DDT}. Shortly after DDT we see the coupling of the shock and flame forming the detonation

wave.

4.1.4 Methane-Air Experimental Comparison

We can use the results of methane-air mixtures for comparison with other codes as well as experimental data. Previous work performed for channels with periodic obstacles detailed in Section 4.1.1 shows good agreement with simulation predictions. Additionally, the results obtained using FAST are compared to another reactive fluid code ALLA described in [45]. FAST and ALLA computations are compared with experimental results from Kuznetsov et al. [1] and Zipf et al. [2]. Simulations show good agreement up to DDT. Additionally, estimates on L_{DDT} in experimental data sets is poor due to lack of spatial resolution. For large scale ($D > 1m$), limited experimental data exists. The accuracy of the simulations can be increased as results for methane-air DDT become available.

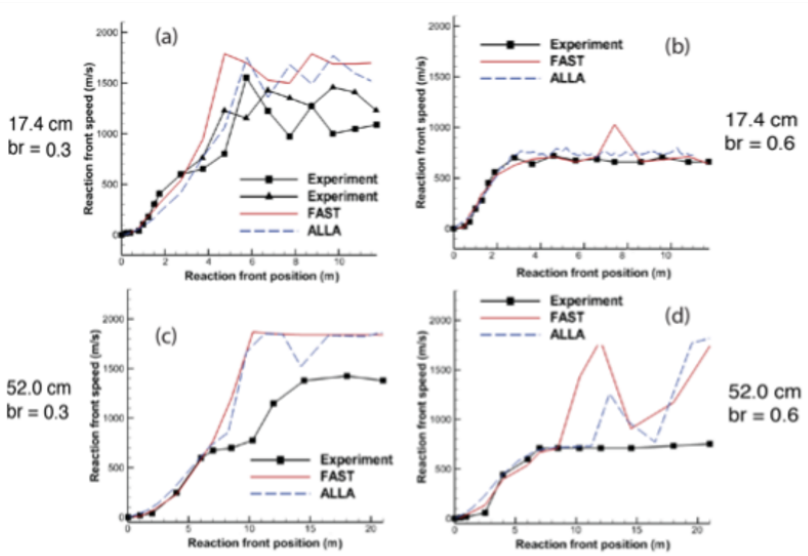

Figure 4.11: DDT comparison with FAST, ALLA, and Zipf et al. [2]

We also see good agreement with experimental measurements with tubes of varying diameter. Both codes FAST and ALLA show close predictions of L_{DDT}. The variance in computational and experimental measurements is comparable to the degree of uncertainty in the experimental data.

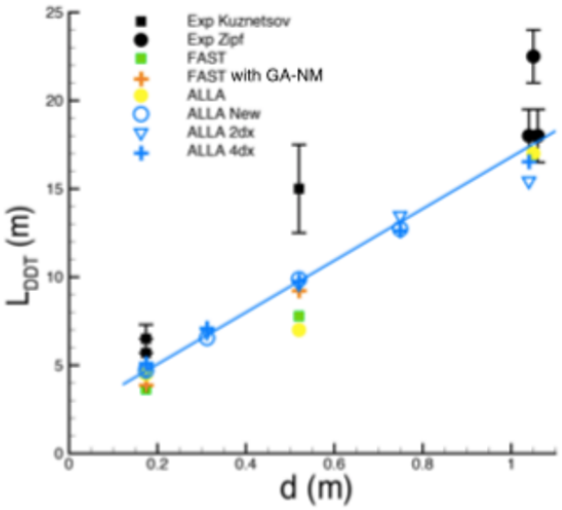

Figure 4.12: DDT scaling comparison with ALLA and Zipf et al. [2] and Kuznetsov et al. [1]

4.1.5 Effect of Impurities

We repeated the simulation for each methane-air mixture containing various amounts (0%, 1%, 2%, 4%, 6%, 8%) of heavy hydrocarbon impurity at each channel size ($D = 17cm$, $D = 32cm$, $D = 1m$). For all mixture compositions, we see a linear trend in L_{DDT} increase for channel size. As the channel diameter increases, we see a corresponding linear increase in the length and time for DDT onset.

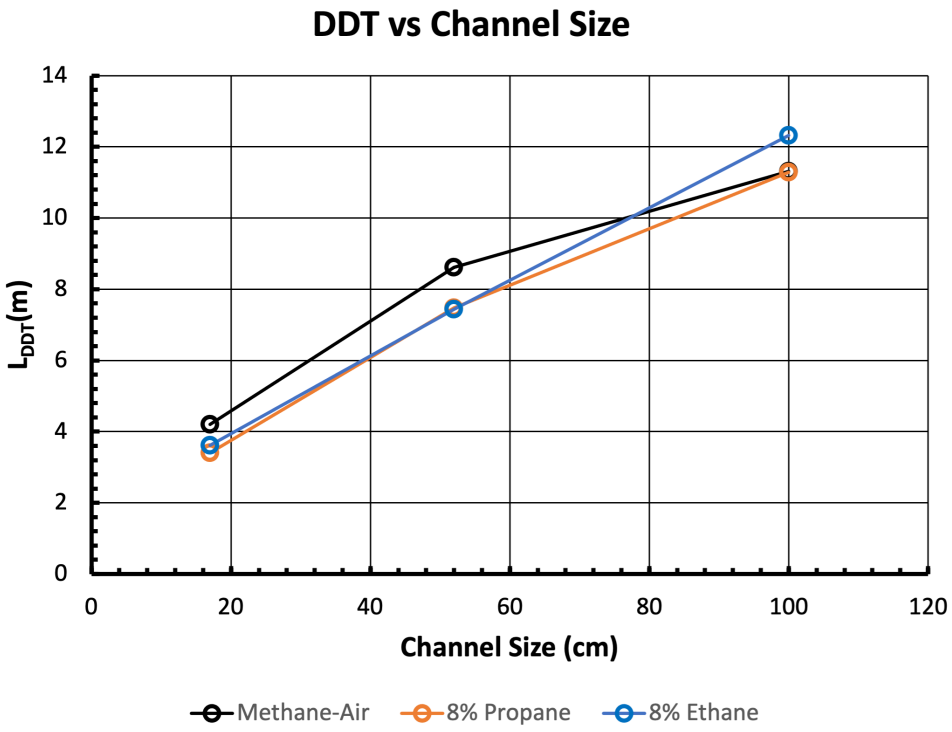

Figure 4.13: Geometric scaling effects

While these simulations are technically determinant, we can induce a degree of stochasticity by varying the initial temperature by a fraction of a degree ($0.001K$). This should be impreceivable to the simulation, but should inform us of the stochastic nature of the simulation. Multiple simulations for each configuration were performed only varying the initial temperature of the from $293K \pm 0.002K$. For the 17.4cm channel, we see large variations in L_{DDT}.

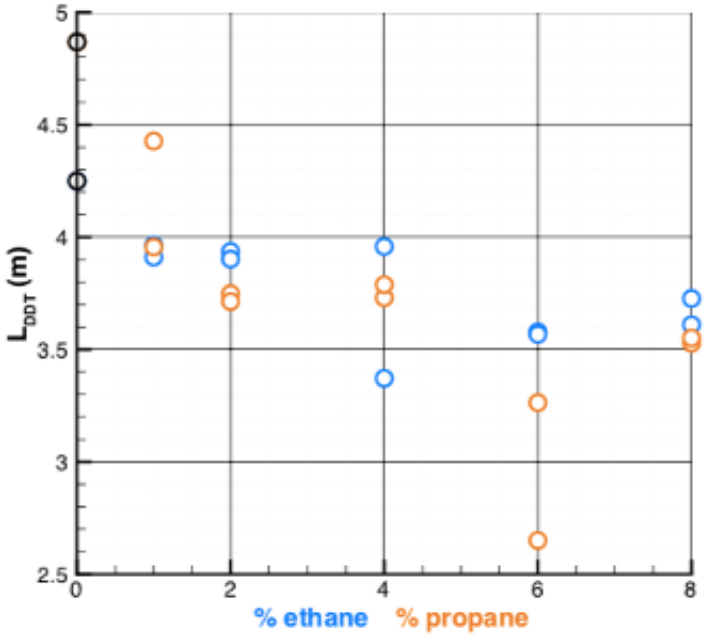

Figure 4.14: Stochasticity of 17.4cm channel

Visualizing L_{DDT} for all channel sizes we see similar scatter and variation in the length it takes for DDT onset.

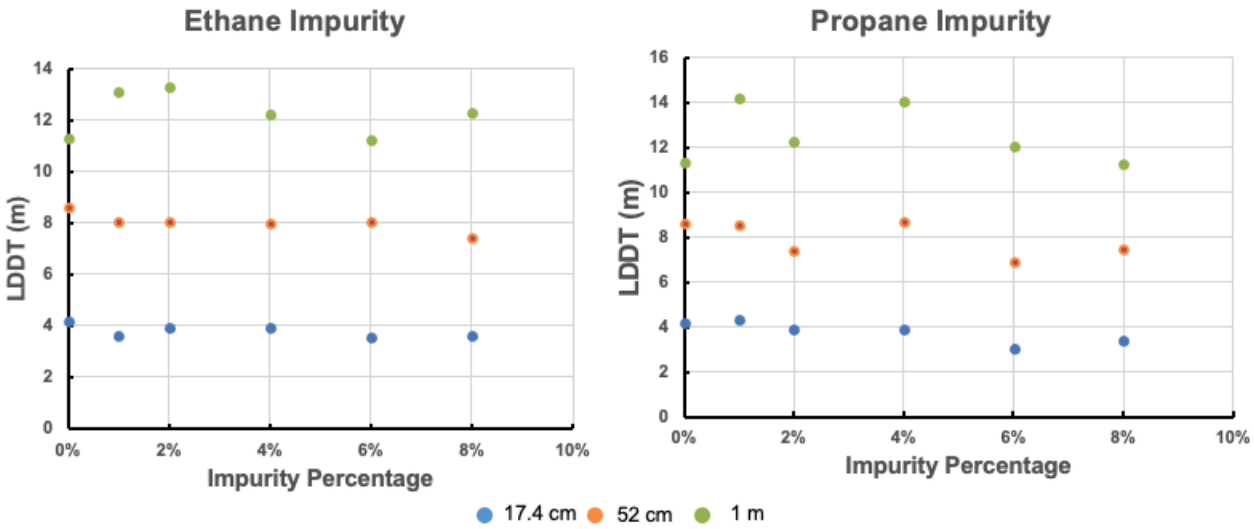

Figure 4.15: Geometric scaling effects of L_{DDT}

The numerical simulations show L_{DDT} for blended mixtures contained in channels with periodic obstacles, and found that the effect of ethane or propane concentration on L_{DDT} is relatively weak and difficult to estimate due to stochastic variations of L_{DDT}. For 17.4cm channel, both ethane and propane seem to reduce L_{DDT} by about the same 15% at a concentration of 2%, and by 20% at a concentration of 8%. For larger channels, the scatter increases, and the data does not show a clear trend.

4.2 Channels with Rubble

4.2.1 Problem Setup

Motivated by the large degree of stochasticity in the simulations of channels with obstacles, we performed simulations on configurations with more regular obstacles to promote consistent turbulence generation. This configuration with small obstacles spaced relatively close together would be similar to a rock rubble pile often found in mines . A flame is ignited at distinct points on the left end of the domain and allowed to propagate through the rubble. Here the channel diameter $d = 32cm$ with rubble spacing $r = s = d/8$. A $BR = 1$ means the entire channel is filled with rubble.

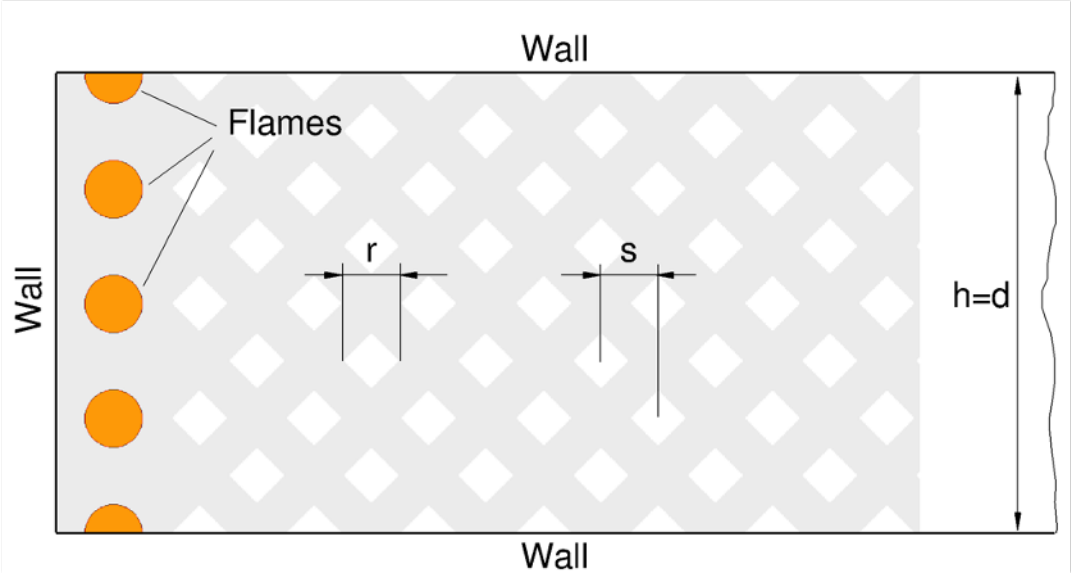

Figure 4.16: Computational domain for channels with rubble

4.2.2 Rubble Results

Similar to channels with periodic obstacles, we see the same flame acceleration, DDT, and detonation through the rubble pile.

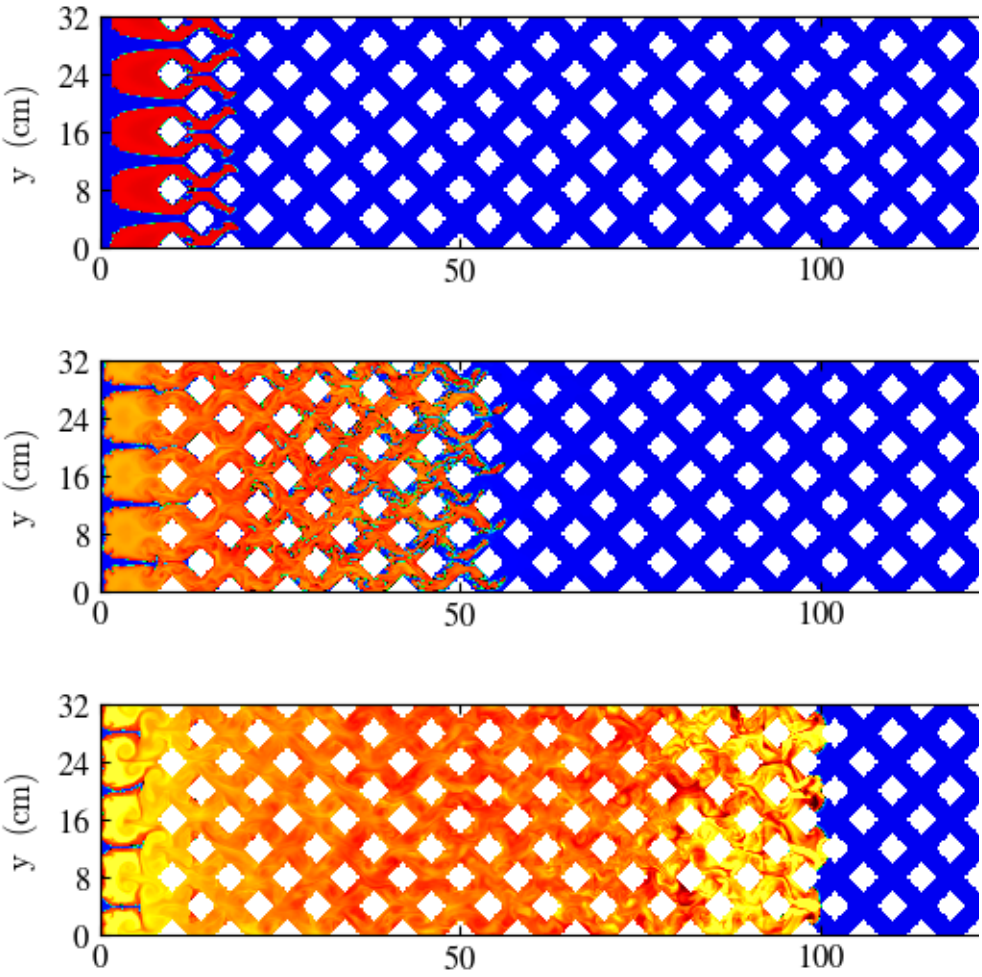

Figure 4.17: Flame propagation through a channel with rubble

Following the same procedure for tracking flame speed as before, we can denote the distance to DDT (L_{DDT}) from simulation diagnostics.

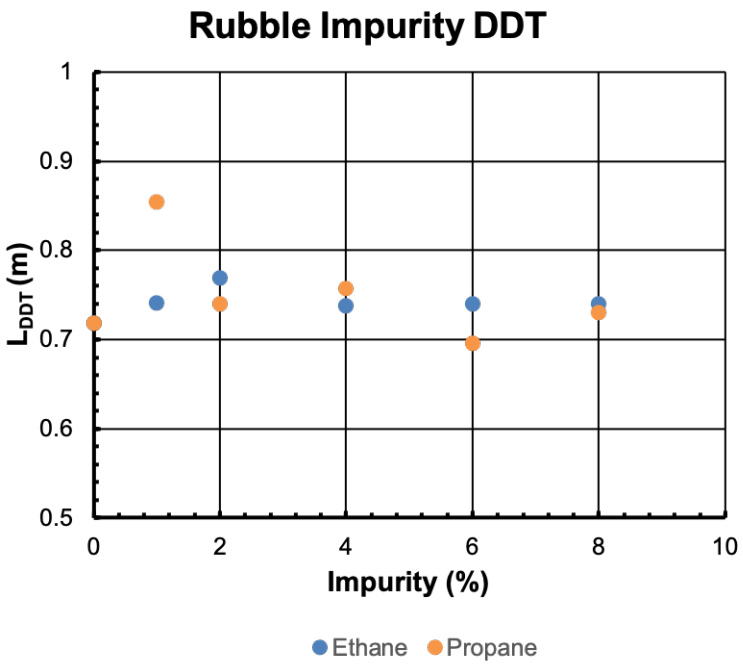

Figure 4.18: L_{DDT} for channels with rubble

For such configurations, we see little change in L_{DDT} for the addition of heavier hydrocarbons. The variance shown is similar to the uncertainty due to turbulence. These results show similar trends to the previous studies on channels with periodic obstacles. This gives strong evidence the addition of alkane impurities in methane-air mixtures has little impact of the distance to DDT.

5. DISCUSSION AND CONCLUSION*

5.1 Discussion

The results for DDT in both channels with periodic obstacles and rubble configurations show the DDT process has little dependence on the inclusion of trace hydrocarbon impurity. This is consistent with the fact that small ethane or propane concentrations have little effect on the laminar flame speed and flame temperature in the resulting mixture. For example, increasing the propane concentration from 0 to 8% increases the laminar flame speed S_l of the stoichiometric methane-propane-air mixture by 6.5% while the flame temperature T_b varies by about 1% generally in the opposite direction. Since S_l and T_b control the flame evolution for the most part of L_{DDT} in obstructed channels, the resulting effect of propane concentration on L_{DDT} is small. On the other hand, the same increase in propane concentration from 0 to 8% decreases the length of the reaction zone in a detonation wave x_d by a factor of 2.8. This should facilitate the shock-induced ignition that is involved at the last stages of DDT, but these last stages are very short compared to the preceding flame evolution in obstructed channels, and thus have little effect on L_{DDT}. We see similar but less drastic trends for ethane addition.

*Parts of this section is reprinted from "Numerical simulation of methane-air DDT in channels containing trace amounts of impurities" with permission from Kunka, L.N., Proceedings of the Mary Kay O'Connor Process Safety Symposium, College Station, TX, 2020, and from "Numerical simulations of flame acceleration and DDT in natural gas: the effects of trace propane and ethane" with permission from Kunka, L.N., 2020 American Physical Society Division of Fluid Dynamics, Chicago, IL, 2020.

Propane

Impurity	$S_L(cm/s)$	$D_{CJ}(m/s)$	$T_b(K)$	$x_{ft}(cm)$	$x_d(cm)$
0%	37.7	1800	2229	0.0448	1.67
1%	38.63	1813	2225	0.0434	1.276
2%	39.03	1807	2234	0.0435	1.056
4%	39.81	1822	2234	0.0442	0.817
6%	39.98	1813	2225	0.0417	0.678
8%	40.17	1828	2206	0.0409	0.591

Table 5.1: Methane-air-propane mixture characteristics

Ethane

Impurity	$S_l(cm/s)$	$D_{CJ}(m/s)$	$T_b(K)$	$x_{ft}(cm)$	$x_d(cm)$
0%	37.7	1800	2224	0.0446	1.68
1%	37.08	1806	2229	0.0443	1.423
2%	38.09	1810	2228	0.0441	1.235
4%	38.56	1809	2232	0.0434	0.9602
6%	38.83	1815	2235	0.0431	0.7761
8%	39.07	1817	2233	0.0426	0.6475

Table 5.2: Methane-air-ethane mixture characteristics

We thus conclude that up to 8% concentrations of ethane or propane in blended methane-air mixtures have no practical effect of the distances to DDT in obstructed channels. The estimated L_{DDT} for blended mixtures are basically the same as for pure methane-air. We can also conclude that in the DDT process from flame ignition to DDT onset, the effect of x_d is negligible. The mixtures examined were practically identical, vary only in half reaction thickness, and the effect this had on L_{DDT} was not discernible from the uncertainty due to turbulence. In fact, the effect of variance in initial temperature ($\pm 0.001K$) has similar effects on L_{DDT}.

These results have several practical considerations. For combustion modeling focusing on laminar flames and acceleration up to DDT, simplified chemical models for methane-air shoud adequately represent realistic natural gas. These models do not need to accurately match ignition delay and induction length. This is not the case for the detonative mode of combustion. The reduced half reaction thickness (x_d) does give indication of a large reduction of cell size in propagating detonation waves. The impurities have a stabilizing effect on the detonation wave, by decreasing the ignition delay. Pure methane versus realistic natural gas mixtures could have large qualitative differences, making natural gas more suitable for practical applications. For example, detonation based systems operating on natural gas could use drastically smaller characteristic lengths.

5.2 Conclusion

Numerical simulation of DDT in methane filled channels with trace percentage (0%-8%) propane or ethane showed little effect on reduce the run up distance to detonation (L_{DDT}). The the variance in L_{DDT} is on the order of the stochasticity of the simulations (variance do to turbulence and turbulence-shock interactions). Hydrodynamics scaled linearly with channel diameter, but the chemical models did not scale with larger channel diameter. Increased heavy hydrocarbon content slightly reduced the laminar flame speed (S_L) and adiabatic burning temperature (T_b) which are the primary driver in the DDT process. Increased heavy hydrocarbon did increase the half-reaction thickness (x_d) which suggest a smaller detonation cell size and thus a more robust detonation.

REFERENCES

[1] M. Kuznetsov, G. Ciccarelli, S. Dorofeev, V. Alekseev, Y. Yankin, and T. H. Kim, "Ddt in methane-air mixtures," *Shock Waves*, vol. 12, pp. 215–220, 11 2002.

[2] R. K. Zipf, V. N. Gamezo, K. M. Mohamed, E. S. Oran, and D. A. Kessler, "Deflagration-to-detonation transition in natural gas-air mixtures," *Combustion and Flame*, vol. 161, pp. 2165–2176, 2014.

[3] V. N. Gamezo, R. K. Zipf, M. J. Sapko, W. P. Marchewka, K. M. Mohamed, E. S. Oran, D. A. Kessler, E. S. Weiss, J. D. Addis, F. A. Karnack, and D. D. Sellers, "Detonability of natural gas-air mixtures," *Combustion and Flame*, vol. 159, pp. 870–881, 2012.

[4] C. R. Kaplan, A. Özgen, and E. S. Oran, "Chemical-diffusive models for flame acceleration and transition-to-detonation: genetic algorithm and optimisation procedure," *Combustion Theory and Modelling*, vol. 23, pp. 67–86, 2019.

[5] G. Smith, D. Golden, M. Frenklach, N. Moriarty, B. Eiteneer, M. Goldenberg, C. Bowman, R. Hanson, S. Song, W. J. Gardine, V. Lissianski, and Z. Qin, "Gri-mech 3.0."

[6] D. M. Johnson, "The potential for vapour cloud explosions - lessons from the buncefield accident," *Journal of Loss Prevention in the Process Industries*, vol. 23, pp. 921–927, 2010.

[7] D. Johnson and V. Tam, "Why ddt is the only way to explain some vapor cloud explosions," *Process Safety Progress*, vol. 36, pp. 292–300, 9 2017.

[8] J. Taveau, "The buncefield explosion: Were the resulting overpressures really unforeseeable?," *Process Safety Progress*, vol. 31, pp. 55–71, 3 2012.

[9] G. W. McMahon, J. R. Britt, and R. E. Walker, "Methane explosion modeling in the sago mine," *Mining Engineering*, vol. 62, pp. 51–62, 2010.

[10] J. H. S. Lee, *The Detonation Phenomenon*. Cambridge University Press, 2008.

[11] E. S. Oran and V. N. Gamezo, "Origins of the deflagration-to-detonation transition in gas-phase combustion," *Combustion and Flame*, vol. 148, pp. 4–47, 1 2007.

[12] E. S. Oran, "Understanding explosions - from catastrophic accidents to creation of the universe," *Proceedings of the Combustion Institute*, vol. 35, pp. 1–35, 2015.

[13] G. B. Goodwin and E. S. Oran, "Premixed flame stability and transition to detonation in a supersonic combustor," *Combustion and Flame*, vol. 197, pp. 145–160, 11 2018.

[14] H. Xiao and E. S. Oran, "Shock focusing and detonation initiation at a flame front," *Combustion and Flame*, vol. 203, pp. 397–406, 2019.

[15] R. K. Zipf, J. F. Brune, and E. D. Thimons, "Progress toward improved engineering of seals and sealed areas of coal mines," *SME Annual Meeting and Exhibit and CMA's 111th National Western Mining Conference 2009*, vol. 2, pp. 641–651, 2009.

[16] D. A. Kessler, V. N. Gamezo, and E. S. Oran, "Simulations of flame acceleration and deflagration-to-detonation transitions in methane-air systems," *Combustion and Flame*, vol. 157, pp. 2063–2077, 11 2010.

[17] W. Zheng, C. Kaplan, R. Houim, and E. Oran, "Flame acceleration and transition to detonation: Effects of a composition gradient in a mixture of methane and air," *Proceedings of the Combustion Institute*, vol. 37, pp. 3521–3528, 1 2019.

[18] V. N. Gamezo, C. L. Bachman, and E. S. Oran, "Effects of scale of flame acceleration and ddt in obstructed channels," pp. 1–11, 2020.

[19] E. Mallard and H. L. Chatelier, *Recherches expérimentales et théoriques sur la combustion des mélanges gazeux explosives*. H.Dunod et E. Pinat, 1883.

[20] G. Ciccarelli and S. Dorofeev, "Flame acceleration and transition to detonation in ducts," aug 2008.

[21] G. B. Goodwin, R. W. Houim, and E. S. Oran, "Effect of decreasing blockage ratio on ddt in small channels with obstacles," *Combustion and Flame*, vol. 173, pp. 16–26, 2016.

[22] H. Xiao and E. S. Oran, "Flame acceleration and deflagration-to-detonation transition in hydrogen-air mixture in a channel with an array of obstacles of different shapes," *Combustion and Flame*, vol. 220, pp. 378–393, 10 2020.

[23] V. N. Gamezo, T. Ogawa, and E. S. Oran, "Numerical simulations of flame propagation and ddt in obstructed channels filled with hydrogen-air mixture," *Proceedings of the Combustion Institute*, vol. 31 II, pp. 2463–2471, 2007.

[24] V. N. Gamezo, T. Ogawa, and E. S. Oran, "Flame acceleration and DDT in channels with obstacles: Effect of obstacle spacing," *Combustion and Flame*, vol. 155, no. 1-2, pp. 302–315, 2008.

[25] N. Chaumeix, S. Pichon, F. Lafosse, and C. E. Paillard, "Role of chemical kinetics on the detonation properties of hydrogen /natural gas/air mixtures," *International Journal of Hydrogen Energy*, vol. 32, pp. 2216–2226, 2007.

[26] C. K. Law and O. C. Kwon, "Effects of hydrocarbon substitution on atmospheric hydrogen-air flame propagation," *International Journal of Hydrogen Energy*, vol. 29, pp. 867–879, 2004.

[27] G. Cheng, P. Bauer, and R. Zitoun, "Influence of propane additives on the detonation characteristics of h2-air mixtures," *EPJ Applied Physics*, vol. 65, 2014.

[28] R. Sorin, R. Zitoun, and D. Desbordes, "Optimization of the deflagration to detonation transition: Reduction of length and time of transition," *Shock Waves*, vol. 15, pp. 137–145, 6 2006.

[29] B. Zhang, L. Pang, X. Shen, and Y. Gao, "Measurement and prediction of detonation cell size in binary fuel blends of methane/hydrogen mixtures," *Fuel*, vol. 172, pp. 196–199, 5 2016.

[30] E. Petersen, D. Kalitan, S. Simmons, G. Bourque, H. J. Curran, and J. Simmie, "Methane/propane oxidation at high pressures: Experimental and detailed chemical kinetic modeling," *Proceedings of the Combustion Institute*, vol. 31, pp. 447–454, 2 2007.

[31] M. M. Holton, P. Gokulakrishnan, M. S. Klassen, R. J. Roby, and G. S. Jackson, "Autoignition delay time measurements of methane, ethane, and propane pure fuels and methane-based fuel blends," *Journal of Engineering for Gas Turbines and Power*, vol. 132, pp. 1–9, 2010.

[32] J. Huang and W. K. Bushe, "Experimental and kinetic study of autoignition in methane/ethane/air and methane/propane/air mixtures under engine-relevant conditions," *Combustion and Flame*, vol. 144, pp. 74–88, 1 2006.

[33] J. Crane, X. Shi, and H. Wang, "A comparison of methane and natural gas detonation limit behaviors," *AIAA Scitech 2020 Forum*, vol. 1 PartF, pp. 1–8, 2020.

[34] C. T. Bowman, "Chemical kinetics models for complex reacting flows."

[35] D. G. Goodwin, R. L. Speth, H. K. Moffat, and B. W. Weber, "Cantera: An object-oriented software toolkit for chemical kinetics, thermodynamics, and transport processes," 8 2018.

[36] G. B. Goodwin, R. W. Houim, and E. S. Oran, "Shock transition to detonation in channels with obstacles," *Proceedings of the Combustion Institute*, vol. 36, no. 2, pp. 2717–2724, 2017.

[37] R. W. Houim and K. K. Kuo, "A low-dissipation and time-accurate method for compressible multi-component flow with variable specific heat ratios," *Journal of Computational Physics*, vol. 230, pp. 8527–8553, 2011.

[38] E. M. Taylor, M. Wu, and M. P. Martı, "Optimization of nonlinear error for weighted essentially non-oscillatory methods in direct numerical simulations of compressible turbulence," vol. 223, pp. 384–397, 2007.

[39] E. Toro, *Riemann Solvers and Numerical Methods for Fluid Dynamics: A Practical Introduction*. 01 2009.

[40] A. Chaudhuri, A. Hadjadj, and A. Chinnayya, "On the use of immersed boundary methods for shock/obstacle interactions," *Journal of Computational Physics*, vol. 230, pp. 1731–1748, 2011.

[41] J. P. Boris, "On large eddy simulation using subgrid turbulence models comment 1," pp. 344–353, Springer Berlin Heidelberg, 1990.

[42] A. Teodorczyk, "Fast deflagrations and detonations in obstacle-filled channels," *Journal of Power Technologies*, vol. 79, pp. 1–34, 1995.

[43] Zeldovich and Y. B., "On the development of detonation in a nonuniformly heated gas," *Astro. Acta*, vol. 15, pp. 313–321, 1970.

[44] M. Liberman, C. Wang, C. Qian, and J. Liu, "Influence of chemical kinetics on spontaneous waves and detonation initiation in highly reactive and low reactive mixtures," *Combustion Theory and Modelling*, vol. 23, no. 3, pp. 467–495, 2019.

[45] V. N. Gamezo, C. L. Bachman, and E. S. Oran, "Flame acceleration and ddt in large-scale obstructed channels filled with methane-air mixtures," *Proceedings of the Combustion Institute*, 2020.